eLIFE elifesciences.org

RESEARCH ARTICLE

Figures and figure supplements

Key steps in unconventional secretion of fibroblast growth factor 2 reconstituted with purified components

Julia P Steringer *et al*

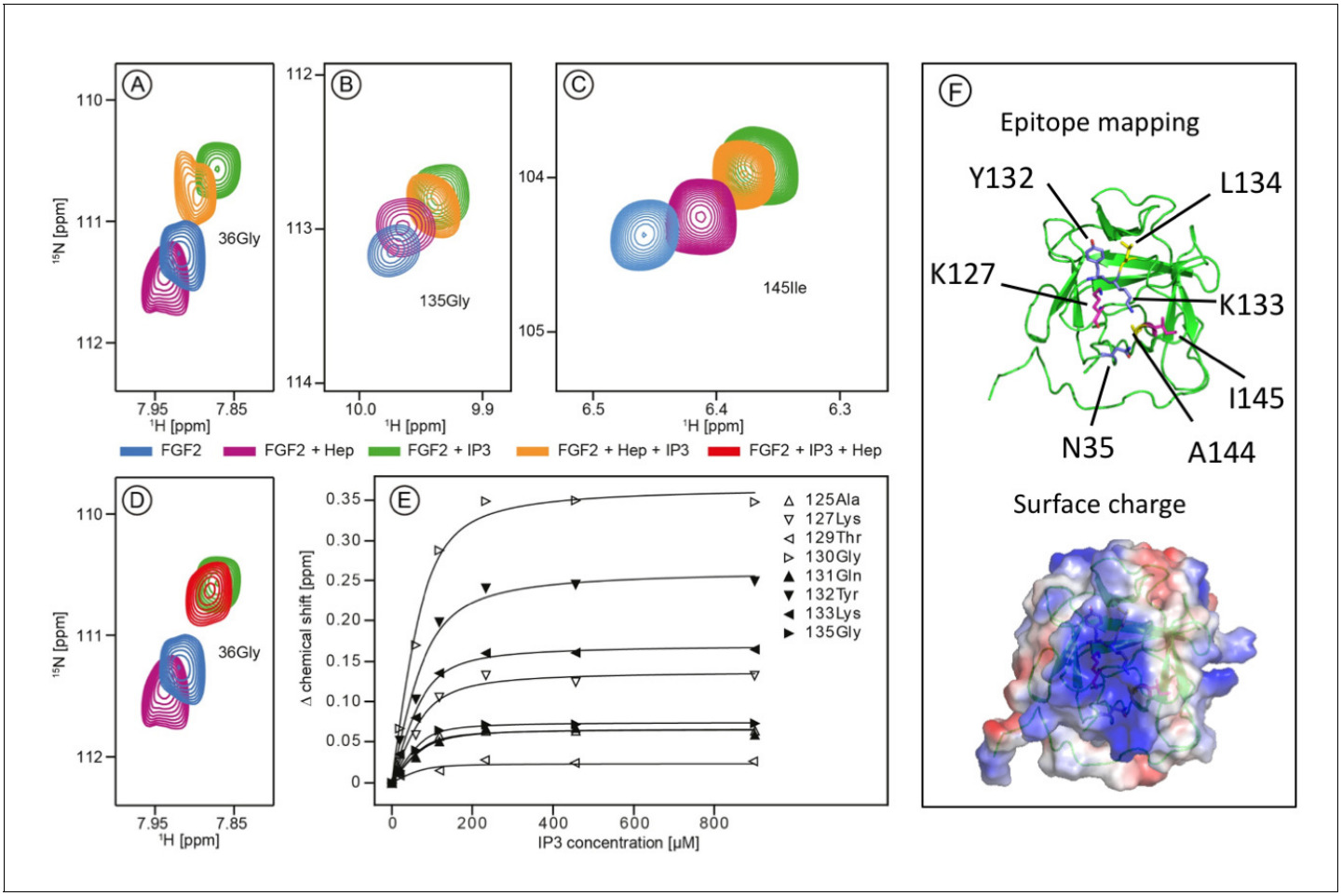

Figure 1. Structural analysis of the FGF2 binding epitopes for IP_3 [head group of $PI(4,5)P_2$] and heparin employing NMR spectroscopy. Enlarged regions of exemplary resonance peaks from a two-dimensional ^{15}N-^{1}H correlation spectrum that are shifted upon addition of IP_3 and Heparin or both are shown on panels (**A** to –**D**). In panel (**E**), titration curves for individual ^{15}N-^{1}H resonances are shown. Binding curves were fitted according to a simple two-state binding model and a K_D was derived from the mean of the individual titration curves. HSQC for all NMR titration experiments are given in ***Figure 1—source data 1***. In panel F (top), a cartoon of the FGF2 NMR structure is shown (PDB: 1BLD) with the side-chain of residues most significantly shifted upon IP_3 binding (blue), heparin binding (yellow) or affected by both binding partners (magenta). In addition, surface mapping of residues shown in panel E using the known structure (PDB: 1BLD) of FGF2 is illustrated in the bottom part of panel (**F**). Both IP_3 and heparin binding epitopes map to the same positively charged region of FGF2 highlighted in blue.

DOI: 10.7554/eLife.28985.002

The following source data is available for figure 1:

Source data 1. Data for ***Figure 1***, panels A-E.

DOI: 10.7554/eLife.28985.003

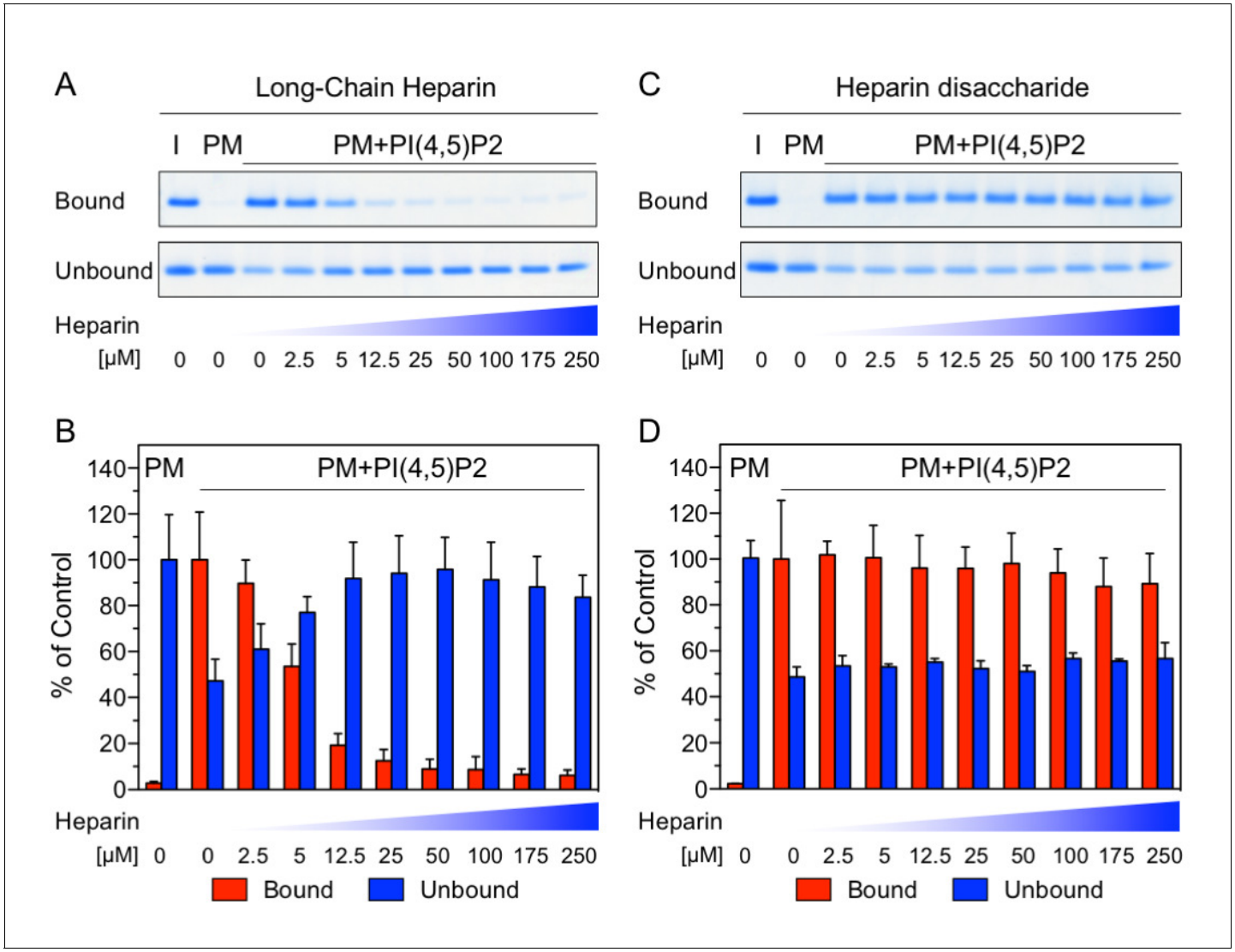

Figure 2. Binding of FGF2 to PI(4,5)P2 and heparin is mutually exclusive. Biochemical analysis employing plasma-membrane-like liposomes either lacking (PM) or containing 2 mol% PI(4,5)P_2 (PM +PIP2). Large unilamellar vesicles (LUVs) with bound His-FGF2-Y81pCMF-WT were incubated with increasing concentrations of either long-chain heparins or a defined heparin disaccharide as indicated. After 1 hr of incubation liposome-associated material (bound) was separated from supernatants (unbound). 50% of bound, 13.5% unbound and 14.8% of input material (I) were analyzed by SDS-PAGE. Coomassie-derived signals were quantified and normalized to controls. The fraction of FGF2-Y81pCMF-WT bound to PM-like liposomes containing PI(4,5)P_2 in the absence of heparin was set to 100% (red bars in ***Figure 2B and D***). The unbound fraction of FGF2-Y81pCMF-WT was normalized using PM-like liposomes lacking PI(4,5)P_2 (blue bars in ***Figure 2B and D***). Mean values with standard deviations are shown (n = 3). Raw and normalized data of individual experiments as well as calculations of mean values with standard deviations are shown in ***Figure 2—source data 1***.

DOI: 10.7554/eLife.28985.004

The following source data is available for figure 2:

Source data 1. Data for ***Figure 2***, panels B and D.

DOI: 10.7554/eLife.28985.005

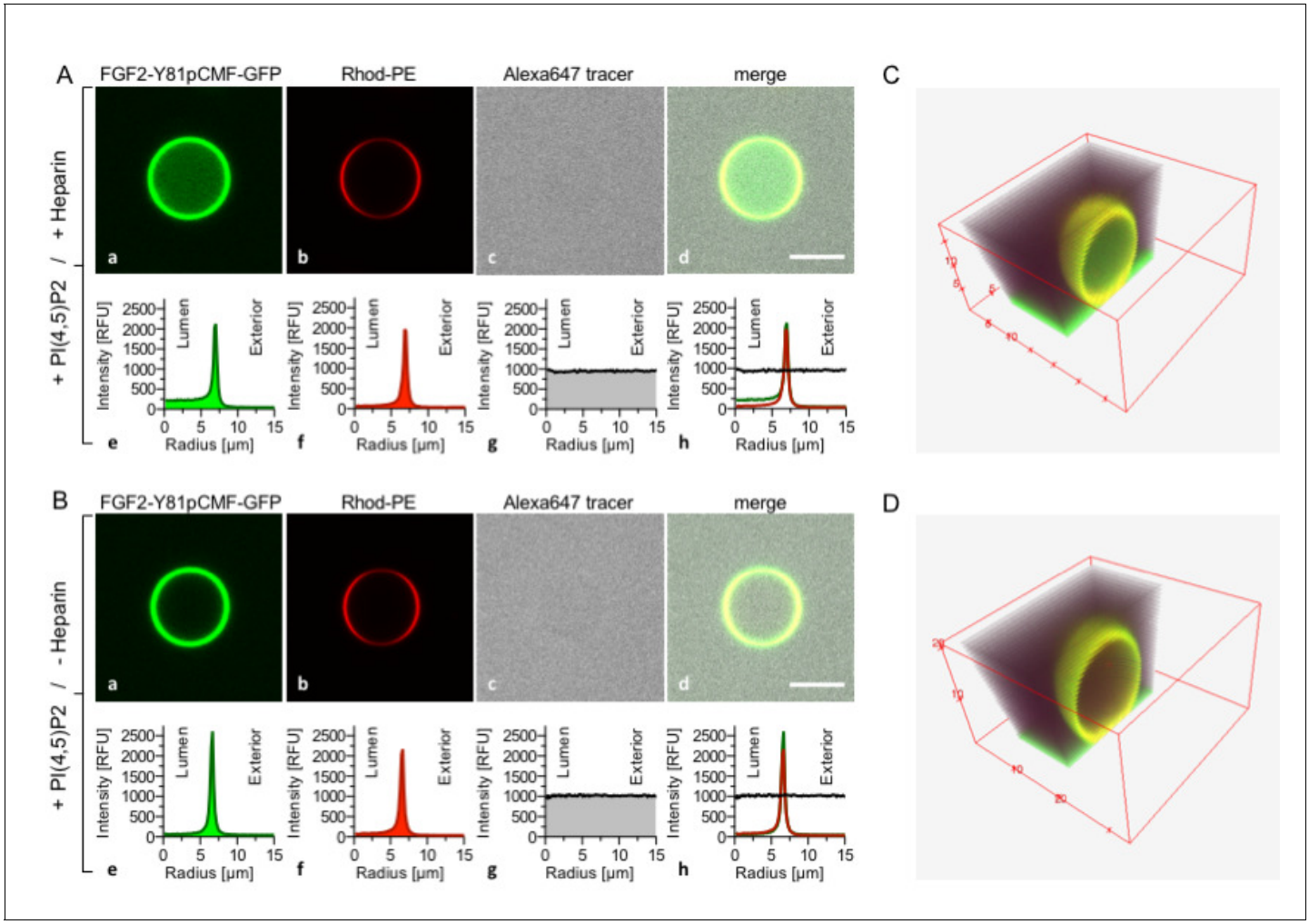

Figure 3. Reconstitution of FGF2 membrane translocation with purified components. Giant unilamellar vesicles with a plasma membrane-like lipid composition containing PI(4,5)P_2 were prepared in the presence (panel **A** and **C**) or absence (panel **B** and **D**) of long-chain heparins. Rhodamine-PE was incorporated into the lipid bilayer during GUV preparation as membrane marker. After removal of excess heparin by low speed centrifugation, GUVs were incubated with FGF2-Y81pCMF-GFP (200 nM) and a small fluorescent tracer (Alexa647). Following 180 min of incubation luminal penetration of GUVs by FGF2-Y81pCMF-GFP and small tracer molecules was analyzed by confocal microscopy (scale bar = 10 µm). GUVs were analyzed in all three channels using the plugin 'Radial profile' of the ImageJ software as explained under 'Materials and methods'. Profile plots of normalized integrated intensities around concentric circles as a function of distance from the center of the GUV are given in relative fluorescence units (RFU). FGF2 membrane translocation is indicated by increased GFP fluorescence intensity in the lumen of GUVs compared to the exterior as exemplified in sub-panel e of panel **A**. The dependence of FGF2-Y81pCMF-GFP membrane translocation on luminal heparin is further documented by 3D reconstruction images (panels **C** and **D**) providing a spatial view into the GUV interior.

DOI: 10.7554/eLife.28985.006

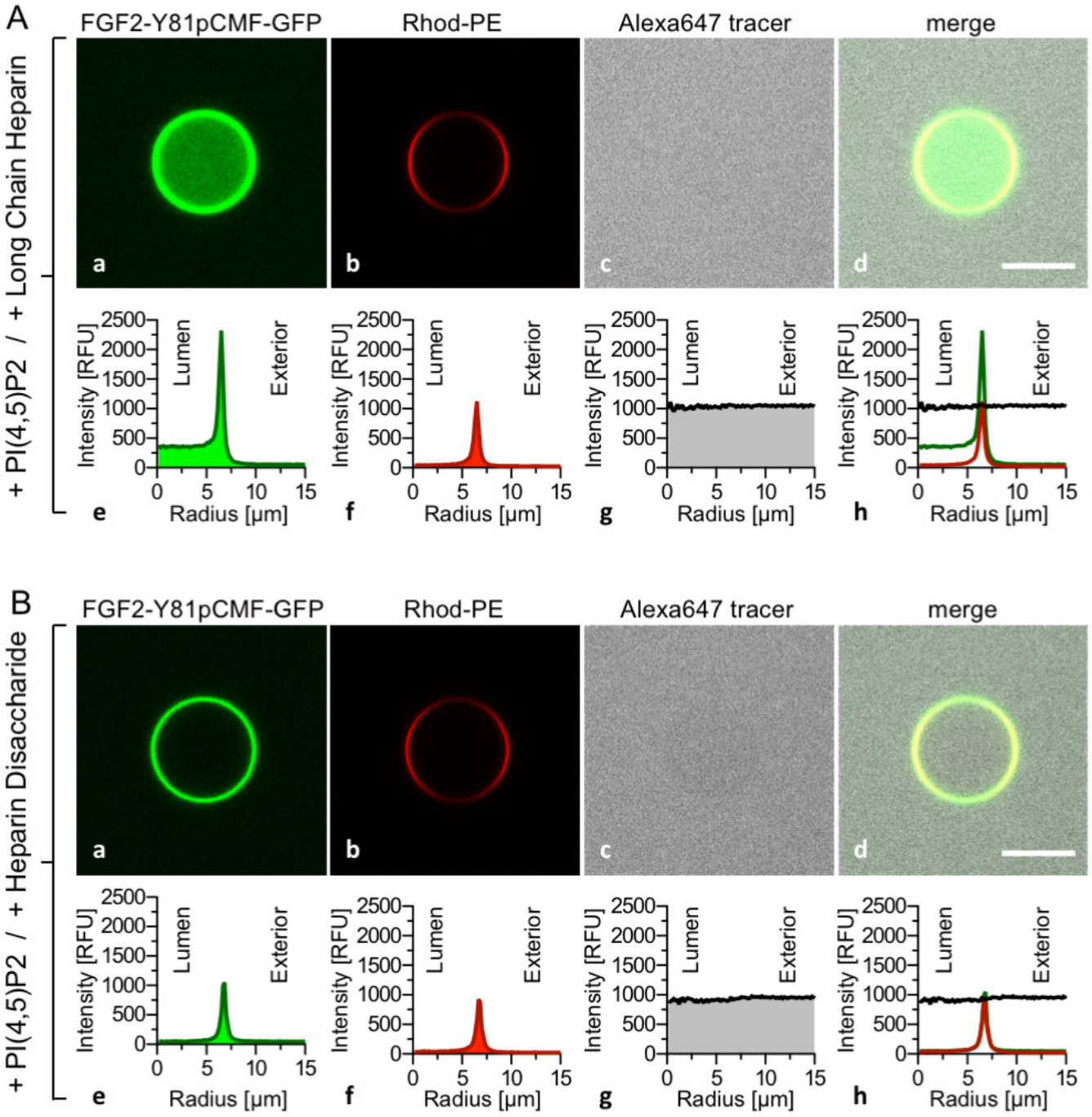

Figure 4. FGF2 membrane translocation depends on luminal long-chain heparins that cannot be substituted by low affinity heparin disaccharides. Giant unilamellar vesicles with a plasma membrane-like lipid composition containing PI(4,5)P_2 were prepared that contain either long-chain heparins (panel A) or a defined heparin disaccharide (panel B). Incubation with FGF2-Y81pCMF-GFP and data analysis were conducted as described in the legend to ***Figure 3*** and under 'Materials and methods'.

DOI: 10.7554/eLife.28985.007

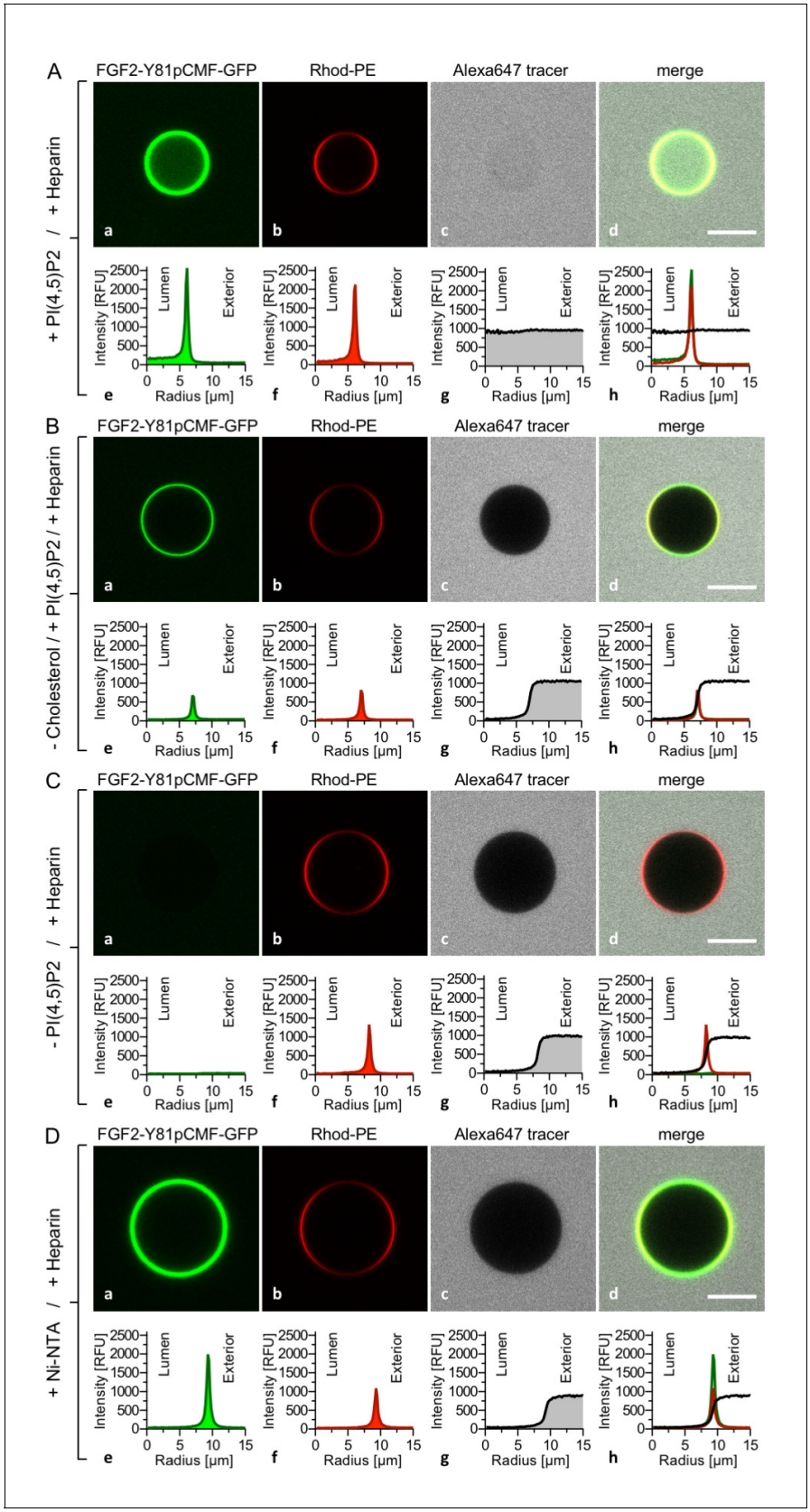

Figure 5. PI(4,5)P_2 is required for both membrane pore formation and FGF2 membrane translocation. Giant unilamellar vesicles were prepared with a plasma membrane-like lipid composition either containing PI(4,5)P_2 (panel **A**), containing PI(4,5)P_2 but lacking cholesterol (panel **B**), lacking PI(4,5)P_2

Figure 5 continued on next page

Figure 5 continued

(panel **C**) or containing a Ni-NTA lipid substituting $PI(4,5)P_2$ (panel **D**). All four types of GUVs contained luminal long-chain heparins. Incubation with FGF2-Y81pCMF-GFP and data analysis were conducted as described in the legend to ***Figure 3*** and under 'Materials and methods'. Note increased GFP fluorescence in the lumen of GUVs as exemplified in sub-panel e of panel A indicating FGF2-Y81pCMF-GFP membrane translocation.

DOI: 10.7554/eLife.28985.008

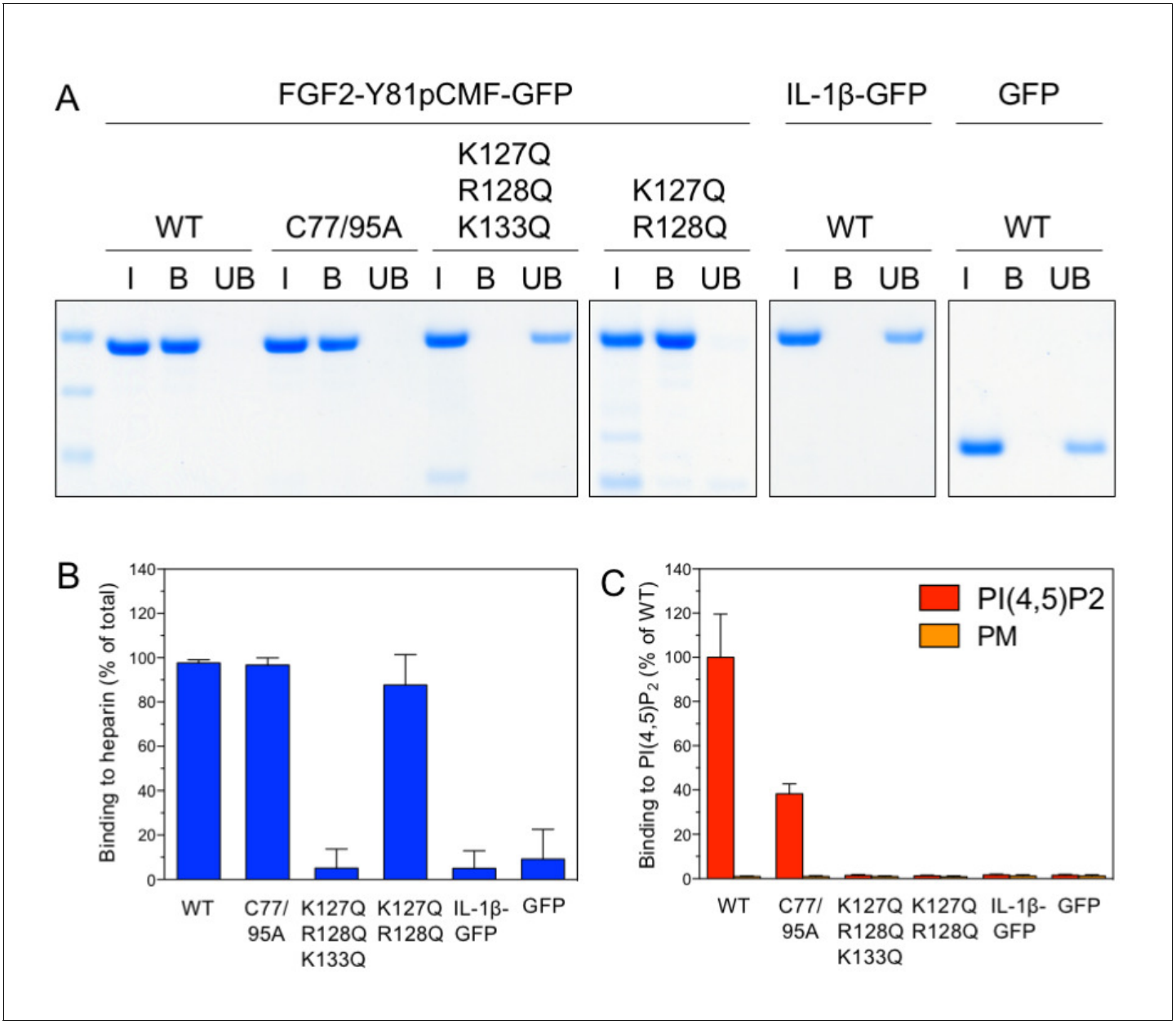

Figure 6. Analysis of FGF2 variant forms with differential defects in binding to PI(4,5)P_2 and heparin. The variant forms of FGF2-Y81pCMF-GFP indicated were tested for binding to heparin beads (panels **A** and **B**) and PI(4,5)P_2 (panel **C**). Heparin sepharose beads were incubated with the FGF2 fusion proteins indicated. Bound and unbound material was separated by centrifugation. Bound proteins were eluted with SDS sample buffer and analysed by SDS-PAGE and Coomassie staining [5% input (I), 20% bound (B) and 5% unbound (UB)]. Signals were quantified using a Li-COR Odyssey infrared imaging system. Mean values with standard deviations of three independent experiments are shown (panel **B**). Raw and normalized data of individual experiments as well as calculations of mean values with standard deviations are shown in ***Figure 6—source data 1***. Binding of the FGF2 fusion proteins to PI(4,5)P_2 contained in plasma membrane-like liposomes was assessed using a flow-cytometry assay (***Temmerman et al., 2008***; ***Temmerman and Nickel, 2009***) (panel **C**). Data were normalized by defining binding of FGF2-Y81pCMF-GFP to PI(4,5)P_2 as 100% binding efficiency. Mean values with standard deviations are shown (n = 4). Consider ***Figure 6—source data 1*** for more details.

DOI: 10.7554/eLife.28985.009

The following source data is available for figure 6:

Source data 1. Data for ***Figure 6***, panels B and C.

DOI: 10.7554/eLife.28985.010

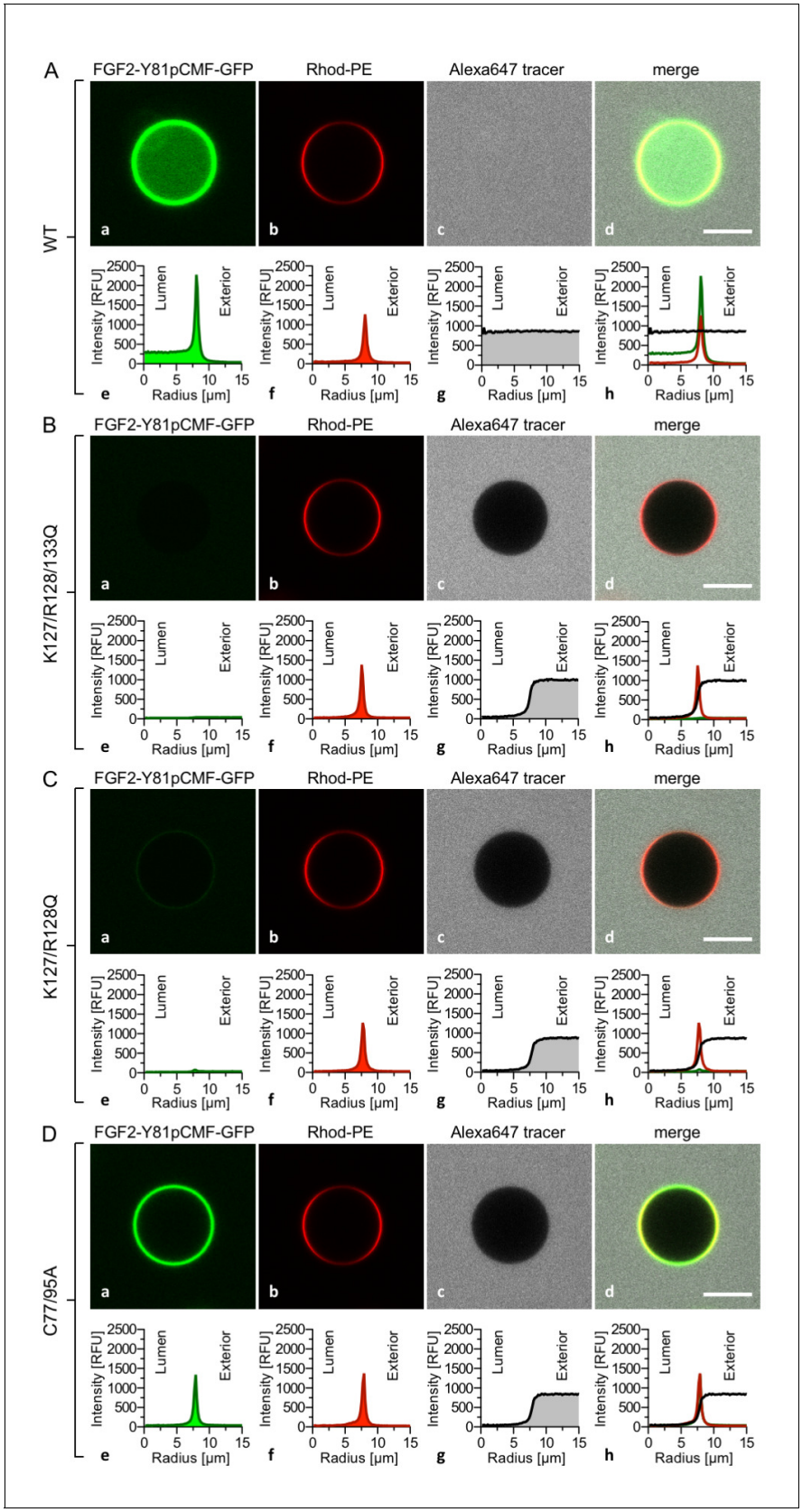

Figure 7. FGF2 membrane translocation depends on *cis*-elements mediating binding to PI(4,5)P_2 and heparin as well as driving FGF2 oligomerization and membrane pore formation. Giant unilamellar vesicles with a plasma membrane-like lipid composition containing both PI(4,5)P_2 and luminal long-

Figure 7 continued on next page

Figure 7 continued

chain heparins were prepared as described in the legend to ***Figure 3*** and under 'Materials and methods'. GUVs were incubated with variant forms of FGF2-Y81pCMF-GFP as indicated. These included the wild-type form (panel **A**), the K127Q/R128Q/K133Q form deficient in binding to PI(4,5)P_2 and heparin (panel **B**), the K127Q/R128Q form deficient in binding to PI(4,5)P_2 (panel **C**) and the C77A/C95A form deficient in oligomerization and membrane pore formation (panel **D**). Incubation conditions and data analysis were conducted as described in the legend to ***Figure 3*** and under 'Materials and methods'. Note increased GFP fluorescence in the lumen of GUVs as exemplified in sub-panel e of panel A indicating membrane translocation of the wild-type form of FGF2-Y81pCMF-GFP.

DOI: 10.7554/eLife.28985.011

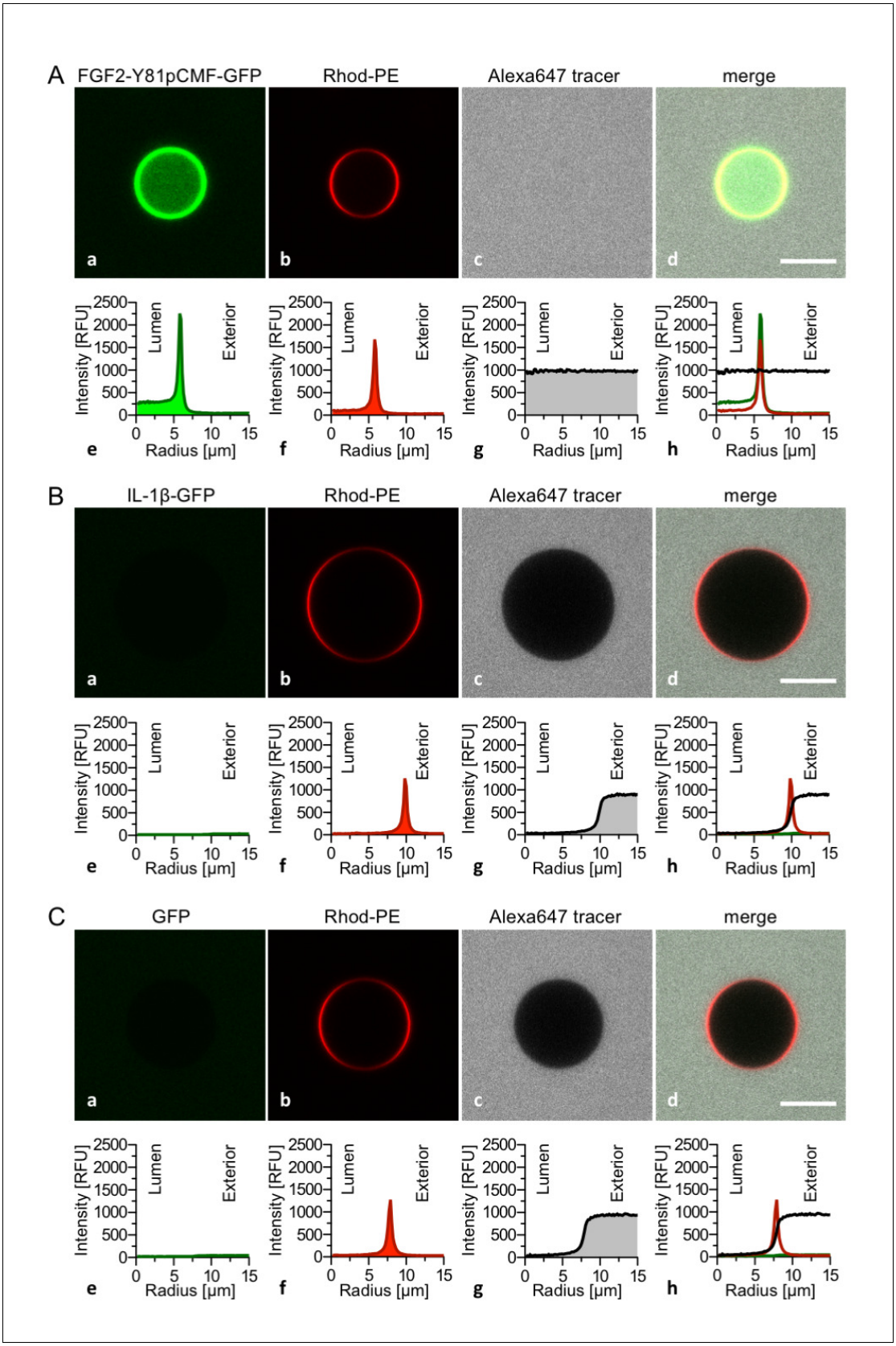

Figure 8. Interleukin 1β, a structural homologue of FGF2, is incapable of binding to PI(4,5)P_2, membrane pore formation and membrane translocation. Giant unilamellar vesicles with a plasma membrane-like lipid composition containing both PI(4,5)P_2 and luminal long-chain heparins were prepared as

Figure 8 continued on next page

Figure 8 continued

described in the legend to ***Figure 3*** and under 'Materials and methods'. Incubation conditions using the wild-type form of FGF2-Y81pCMF-GFP (panel **A**), the mature form of Interleukin 1β-GFP (panel **B**) and GFP as control protein (panel **C**) as well as data analysis were conducted as described in the legend to ***Figure 3*** and under 'Materials and methods'. Note increased GFP fluorescence in the lumen of GUVs as exemplified in sub-panel e of panel **A** indicating membrane translocation of the wild-type form of FGF2-Y81pCMF-GFP.

DOI: 10.7554/eLife.28985.012

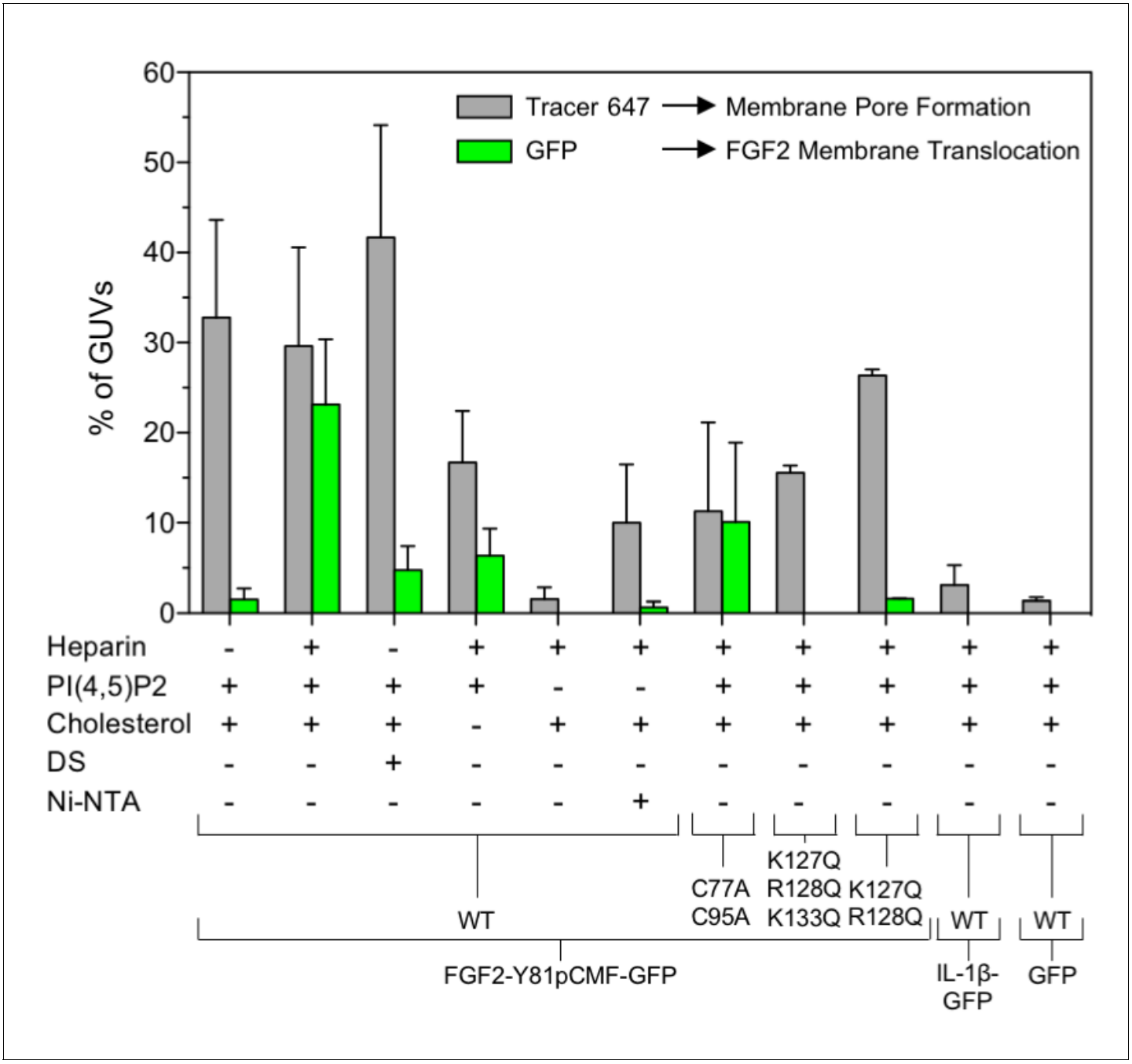

Figure 9. Quantification and statistical analysis of FGF2-Y81pCMF membrane translocation and its dependence on both *cis*-elements and *trans*-acting factors known to be required for FGF2 secretion from cells. A quantitative analysis of membrane translocation and pore formation by the various proteins indicated was conducted based upon the experiments shown in ***Figures 3***, ***4***, ***5***, ***7*** and ***8***. Various types of GUVs with a plasma membrane-like composition were used that differed with regard to the presence of the components indicated. For all conditions, data were derived from at least three independent experiments each of which involved the analysis of 20–120 GUVs per experimental condition. Gray bars indicate the percentage of GUVs with membrane pores with a ratio of Alexa647 tracer fluorescence in the lumen versus the exterior of ≥0.6. Green bars indicate the percentage of GUVs where membrane translocation of GFP-tagged proteins had occurred with a ratio of GFP fluorescence in the lumen versus the exterior of ≥1.6 being used as a threshold value. Standard deviations are shown (n ≥ 15 for experiments shown in ***Figure 3*** and n ≥ 3 for all other conditions shown in ***Figures 4***, ***5***, ***7*** and ***8***). Detailed information on each individual experiment is provided in ***Figure 9—source data 1***.

DOI: 10.7554/eLife.28985.013

The following source data is available for figure 9:

Source data 1. Data for ***Figure 9***.

DOI: 10.7554/eLife.28985.014

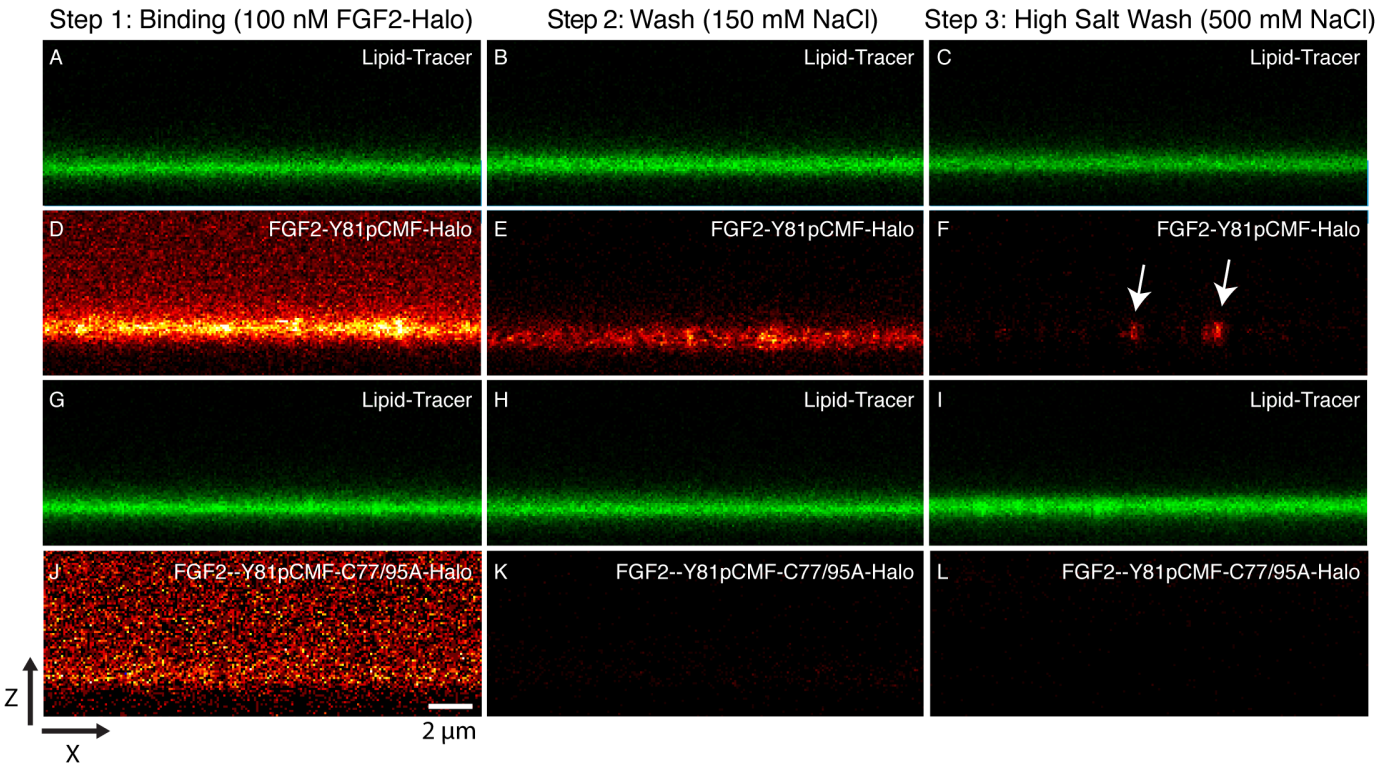

Figure 10. Binding and membrane insertion of FGF2-Halo-StarRed fusion proteins into supported lipid bilayers containing PI(4,5)P_2. FGF2-Y81pCMF-Halo-StarRed (Panels **A–F**) and FGF2-Y81pCMF-C77/95A-Halo-StarRed (panels **G–L**) were added at a final concentration of 100 nM to supported lipid bilayers (SLBs) containing 68 mol% POPC, 30 mol% cholesterol and 2 mol% PI(4,5)P_2 plus trace amounts of DPPE-OregonGreen to image the bilayer. FGF2-Y81pCMF-Halo-StarRed and FGF2-Y81pCMF-C77/95A-Halo-StarRed were bound to SLBs (panels **A, D, G and J**) followed by a 150 mM NaCl washing procedure (panels **B, E, H and K**). In a final step, a 500 mM salt wash was applied to remove FGF2 monomers (panels **C, F, I and L**). FGF2-Y81pCMF-Halo-StarRed and FGF2-Y81pCMF-C77/95A-Halo-StarRed bound to SLBs were imaged as explained in 'Materials and methods'.
DOI: 10.7554/eLife.28985.015

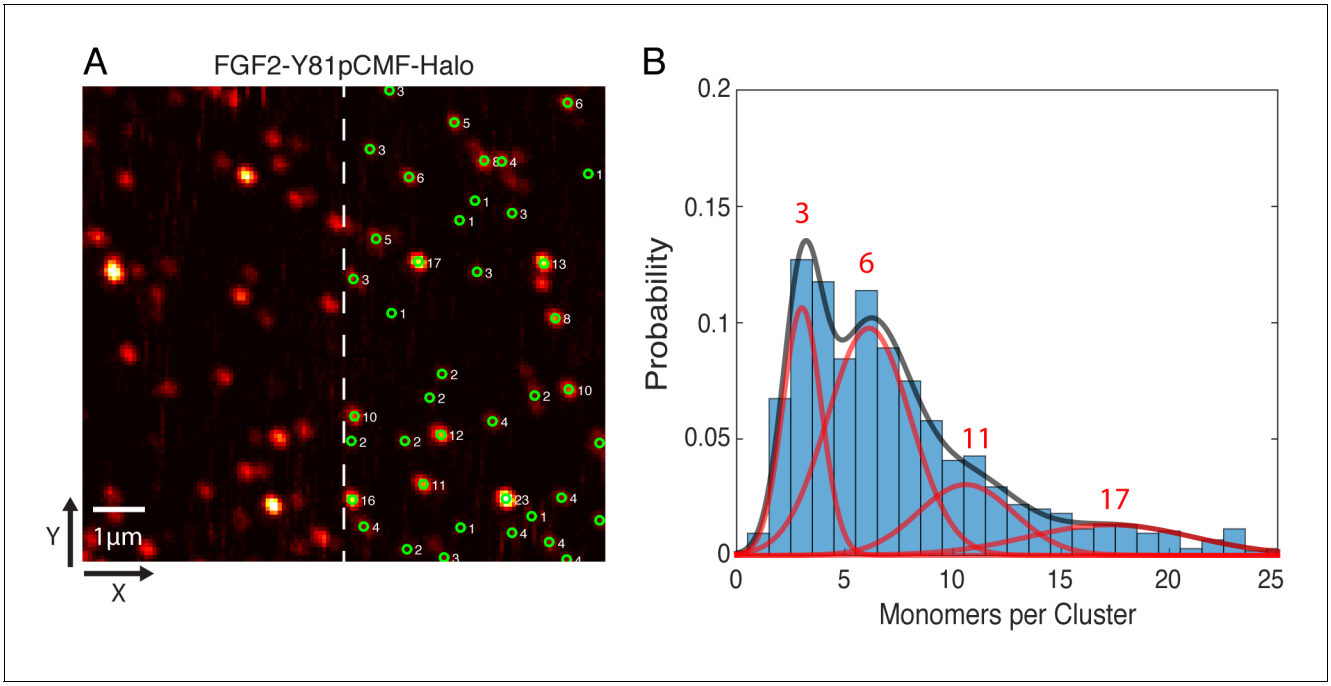

Figure 11. Single molecule imaging and brightness analysis of FGF2-Y81pCMF-Halo-StarRed to determine the oligomeric state of membrane inserted FGF2 clusters. (**A**) Immobile FGF2-Y81pCMF-Halo-StarRed clusters associated with SLBs following a high salt wash (***Figure 10F***) were imaged by confocal microscopy. The brightness of individual clusters was determined by fitting a 2D Gaussian to each diffraction limited spot using a single molecule tracking software in MATLAB. The number of monomers in each cluster (right part of image) was estimated by normalizing the brightness of each cluster to the brightness of monomeric HALO-StarRed). Original peak intensities and cluster analyses are available in ***Figure 11—source data 1***. (**B**) Gaussian mixture analysis of the oligomeric state of membrane inserted FGF2-Y81pCMF-Halo-StarRed (>1000 clusters from six independent experiments). The distribution of monomers per cluster was complex. A Gaussian mixture analysis found 4 components with 3, 6, 11 and 17 monomers per cluster.

DOI: 10.7554/eLife.28985.016

The following source data is available for figure 11:

Source data 1. Data for ***Figure 11***.

DOI: 10.7554/eLife.28985.017

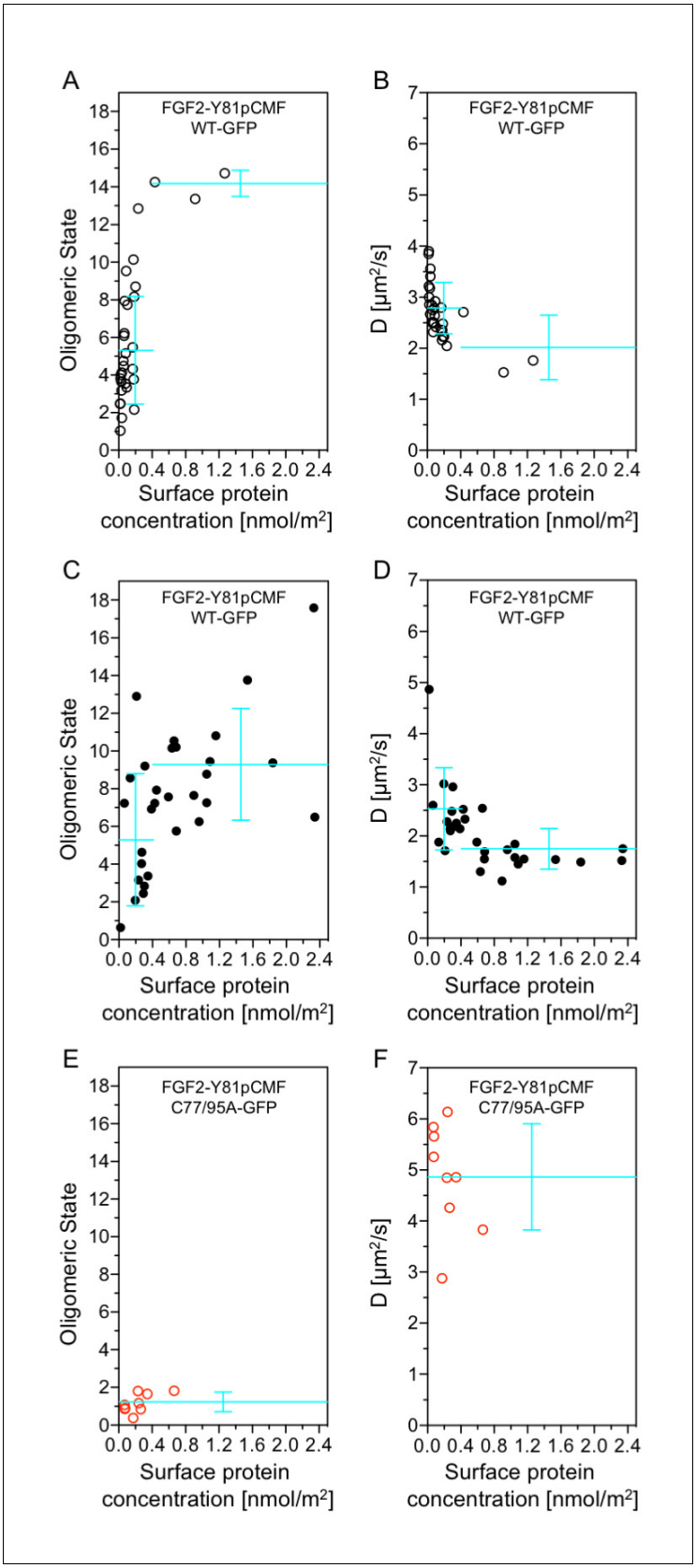

Figure 12. Functional correlation of the oligomeric state of membrane associated FGF2 translocation intermediates and membrane pore formation. Giant unilamellar vesicles with a plasma membrane-like lipid composition containing PI(4,5)P_2 and the membrane tracer DOPE-Atto633 were prepared

Figure 12 continued on next page

Figure 12 continued

as described in 'Materials and methods'. After pre-incubation with either the wild-type form of FGF2-Y81pCMF-GFP (panels **A-D**, black circles) or FGF2-Y81pCMF-C77/95A-GFP (panels **E** and **F**; red circles) for at least 30 min, z-scan FCS measurements using 515/50 nm (FGF2-GFP) and 697/58 nm (DOPE-Atto633) emission channels were conducted on single GUVs. The small free tracer AlexaFlour532 was added to the buffer in order to visualize FGF2 membrane pore formation. Accordingly, GUVs were classified into two groups with (panels **C** and **D**, filled circles) and without membrane pores (panels **A, B, E**, and **F**; empty circles). Z-scan measurements and analyses are described in detail under 'Materials and methods'. Average oligomeric state values (panels **A**, **C, E**) and diffusion constants (panels **B**, **D, F**) were plotted as a function of protein surface concentration. A total of 60 individual GUVs incubated with FGF2-Y81pCMF-WT-GFP (panels **A–D**) and 9 GUVs incubated with FGF2-Y81pCMF-C77/95A (panels **E** and **F**) were analyzed. Additional data of Z-scan FCS for each individual GUV, monomer control reference measurements as well as calculations of mean values with standard deviations are provided in ***Figure 12—source data 1***.

DOI: 10.7554/eLife.28985.018

The following source data is available for figure 12:

Source data 1. Data for ***Figure 12***.

DOI: 10.7554/eLife.28985.019

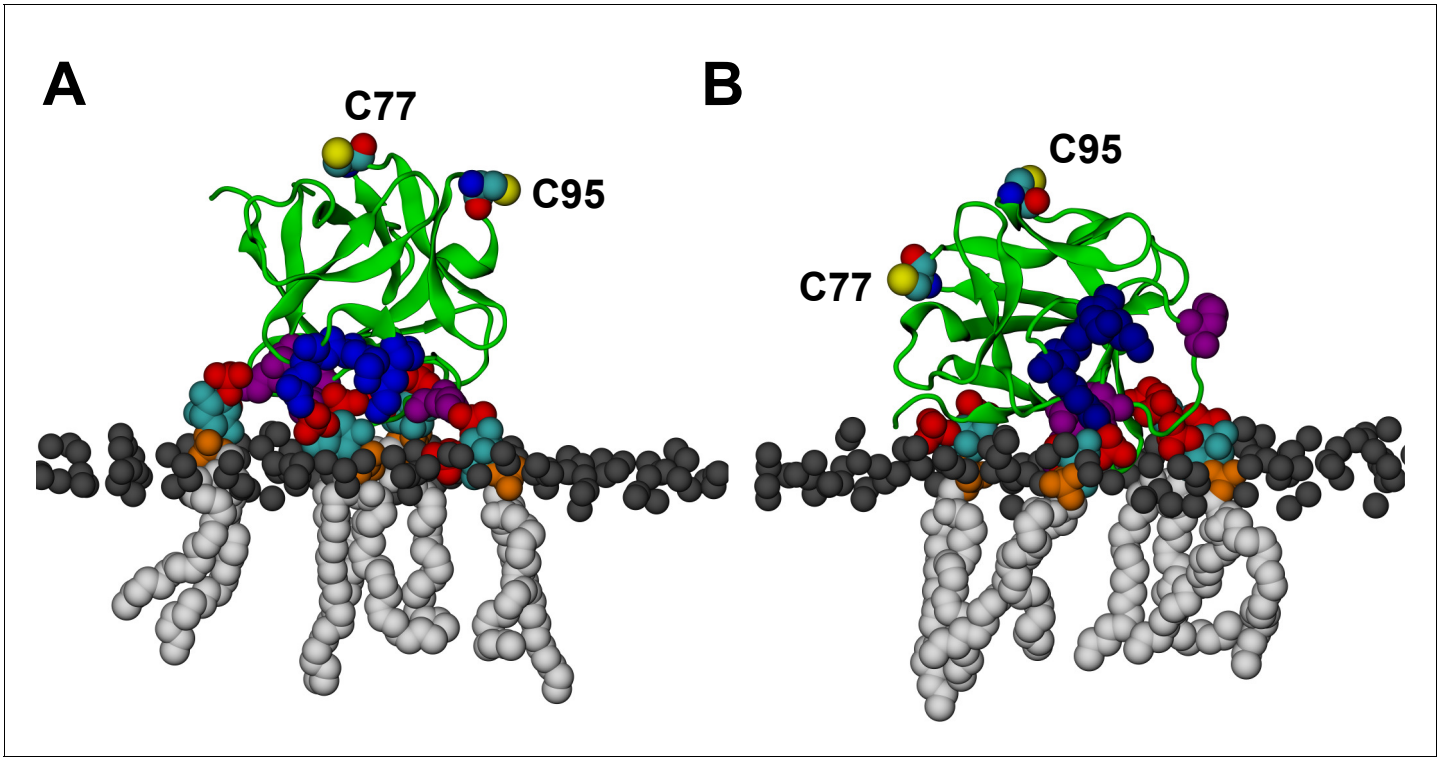

Figure 13. FGF2 orientation on the membrane surface. (**A**) High-affinity orientation of FGF2, showing all the known PI(4,5)P_2-binding site residues (K127, R128, K133) as well as the previously undetermined binding site residues (K34, K137, K143). (**B**) Low-affinity orientation of FGF2 in which the binding site residues lose contact with PI(4,5)P_2 and point away from the PI(4,5)P_2 head groups. FGF2 is rendered as green cartoon, and its C95 and C77 residues are shown as van der Waals (vdW) spheres and highlighted by text in the figure. The key binding pocket residues (K127, R128, K133) are shown as blue vdW spheres, and the additional binding site residues (K34, K137, K143) are shown as purple vdW spheres. Lipids are colored as gray vdW spheres (POPC phosphate atoms), red vdW spheres [PI(4,5)P_2 bisphosphates], cyan vdW spheres [inositol ring in PI(4,5)P_2], orange vdW spheres [phosphate linking the fatty acid chains and the inositol ring in PI(4,5)P_2], and white vdW spheres [fatty acid chains in PI(4,5)P_2]. Water molecules and ions are not shown for clarity.

DOI: 10.7554/eLife.28985.020

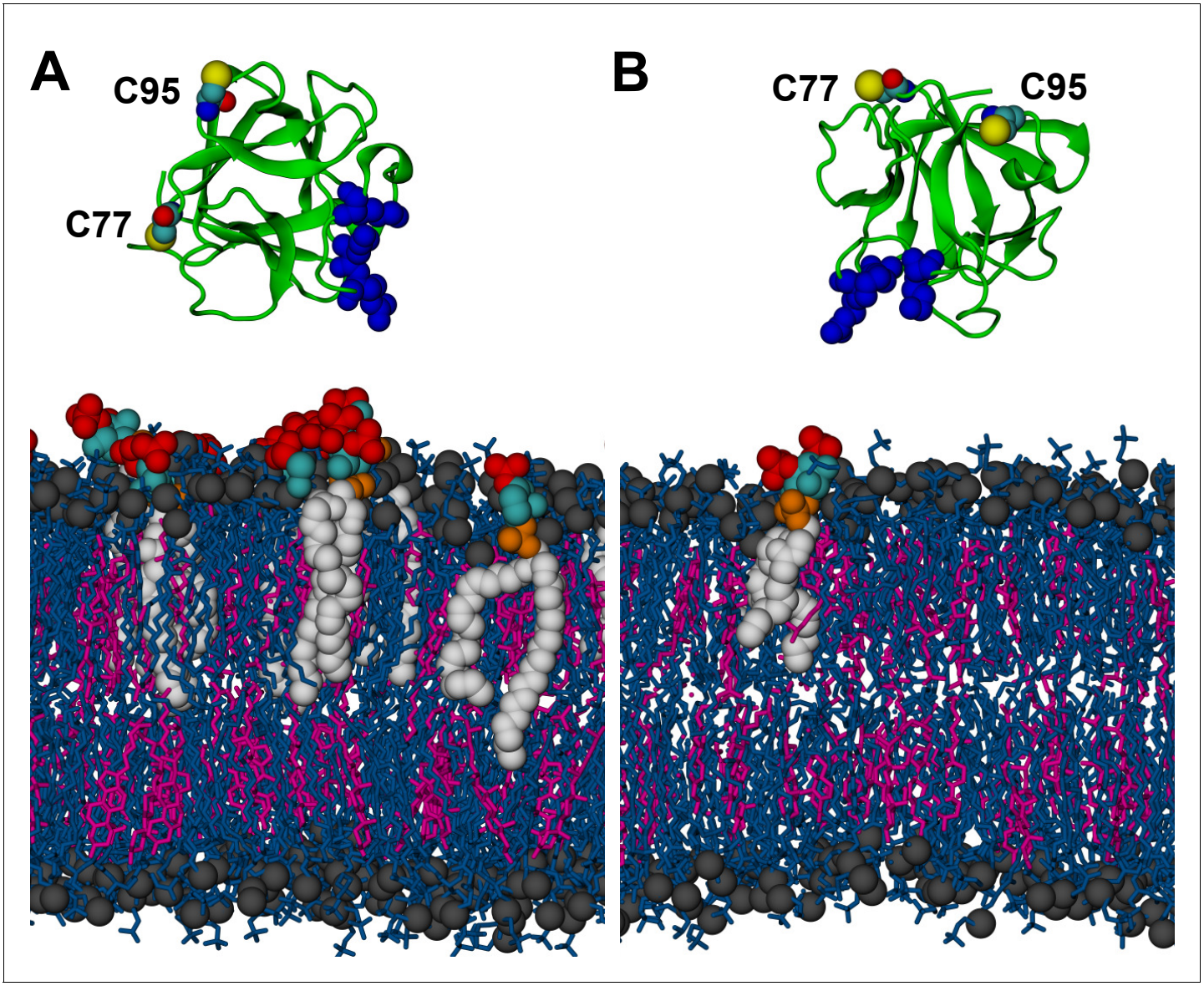

Figure 13—figure supplement 1. Initial structures in systems (A) M1 (POPC/cholesterol/PI(4,5)P_2 (65/29.5/5.5 composition on the cytosolic side interacting with FGF2); see text and ***Table 1***) and (B) M2 (a single PI(4,5)P_2 molecule allowed to interact with FGF2). FGF2 is rendered as green cartoon, C95 and C77 residues are shown as van der Waals (vdW) spheres, and binding pocket residues (K127, R128, K133) are shown as blue van der Waals spheres. Lipids are colored as gray vdW spheres (POPC phosphate atoms), blue licorice (rest of POPC), magenta (cholesterol), red vdW spheres [PI(4,5)P_2 bisphosphates], cyan vdW spheres [inositol ring in PI(4,5)P_2], orange vdW spheres [phosphate linking the fatty acid chains and the inositol ring in PI(4,5)P_2], and white vdW spheres [fatty acid chains in PI(4,5)P_2]. Water molecules and ions are not shown for clarity.

DOI: 10.7554/eLife.28985.021

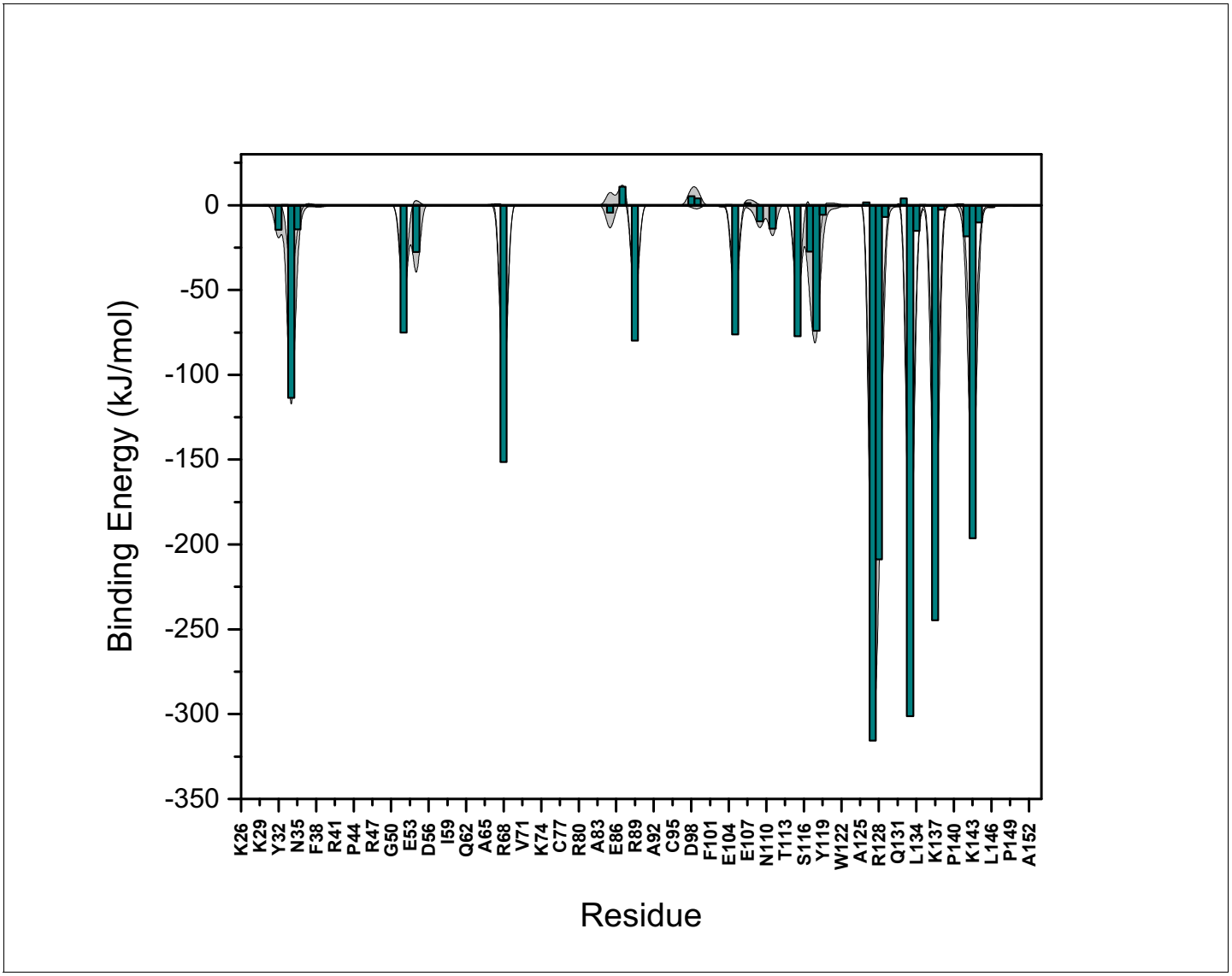

Figure 13—figure supplement 2. PI(4,5)P_2 binding energy based on electrostatics and van der Waals interactions. The average interaction energy (electrostatic and van der Waals contributions) of PI(4,5)P_2 in system M1 over the residues of FGF2 in the high-affinity orientation binding to PI(4,5)P_2. The standard errors are shown as shadows.

DOI: 10.7554/eLife.28985.022

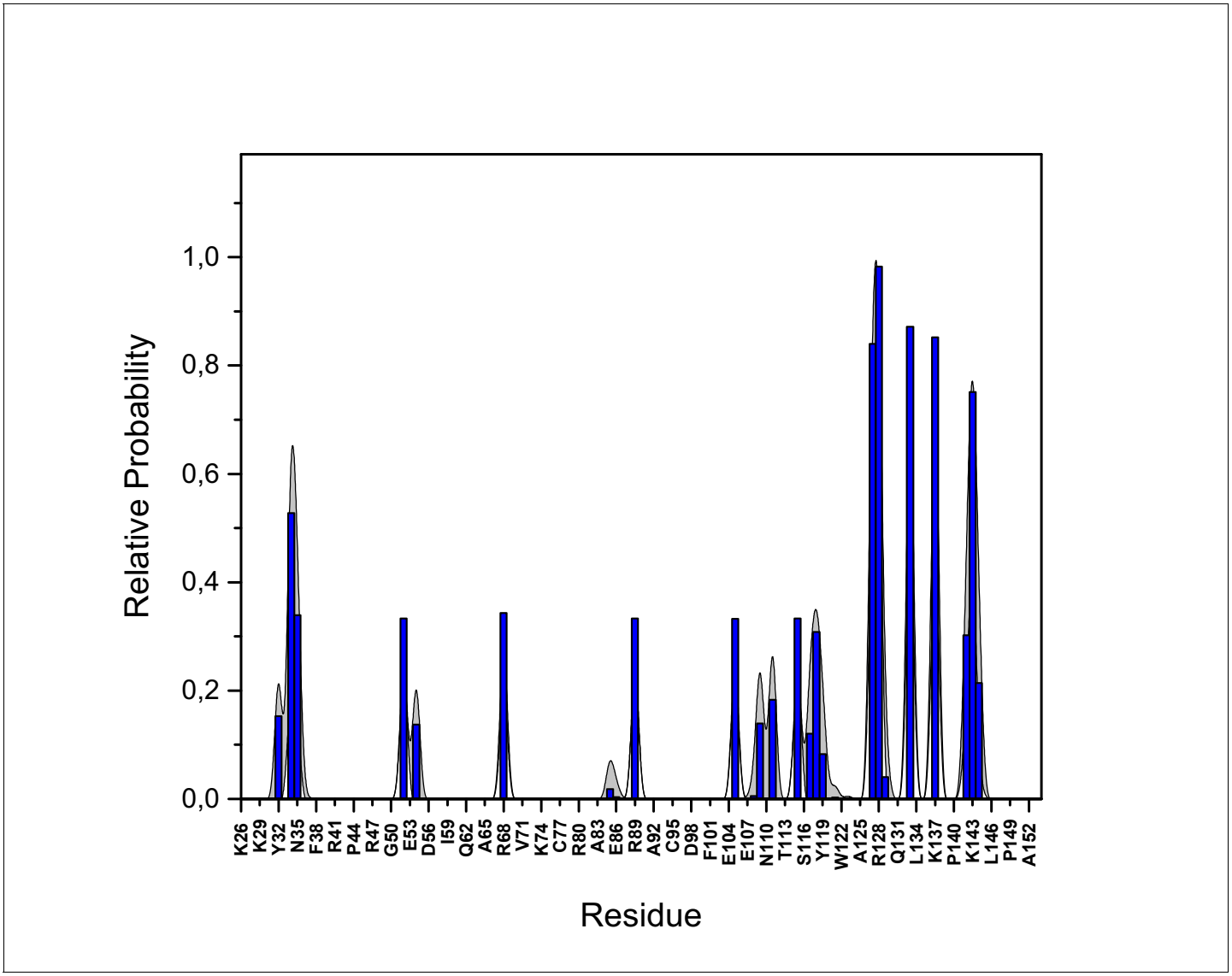

Figure 13—figure supplement 3. PI(4,5)P_2 interaction based on hydrogen bond analysis. Relative probability of hydrogen bonds formed between the residues of FGF2 in the high-affinity orientation and PI(4,5)P_2 (system M1). The standard errors are shown as shadows.
DOI: 10.7554/eLife.28985.023

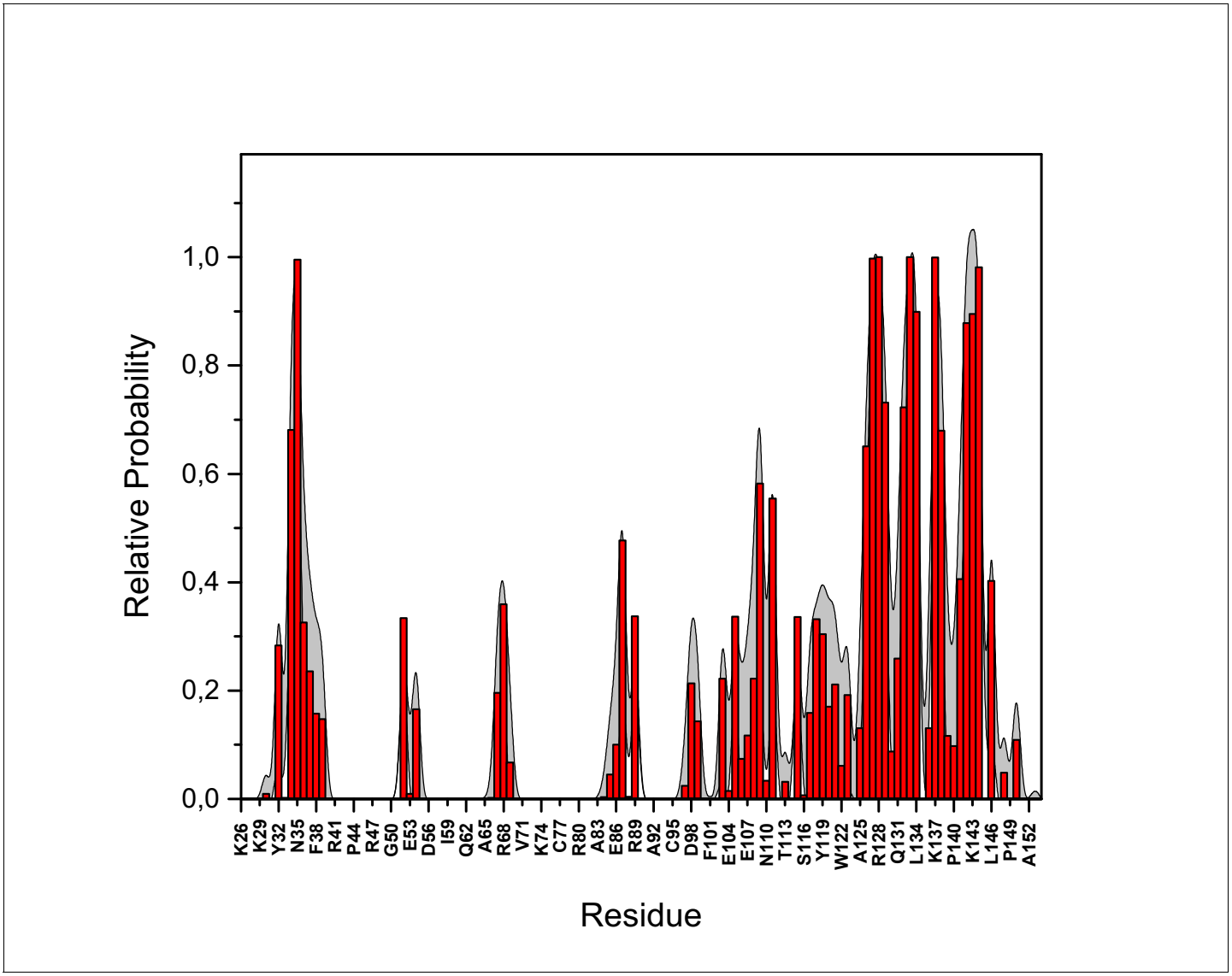

Figure 13—figure supplement 4. PI(4,5)P_2 contacts with FGF2. Relative probability of contacts (<0.6 nm) between the FGF2 residues and PI(4,5)P_2 in the high-affinity orientation (system M1). The standard errors are shown as shadows.
DOI: 10.7554/eLife.28985.024

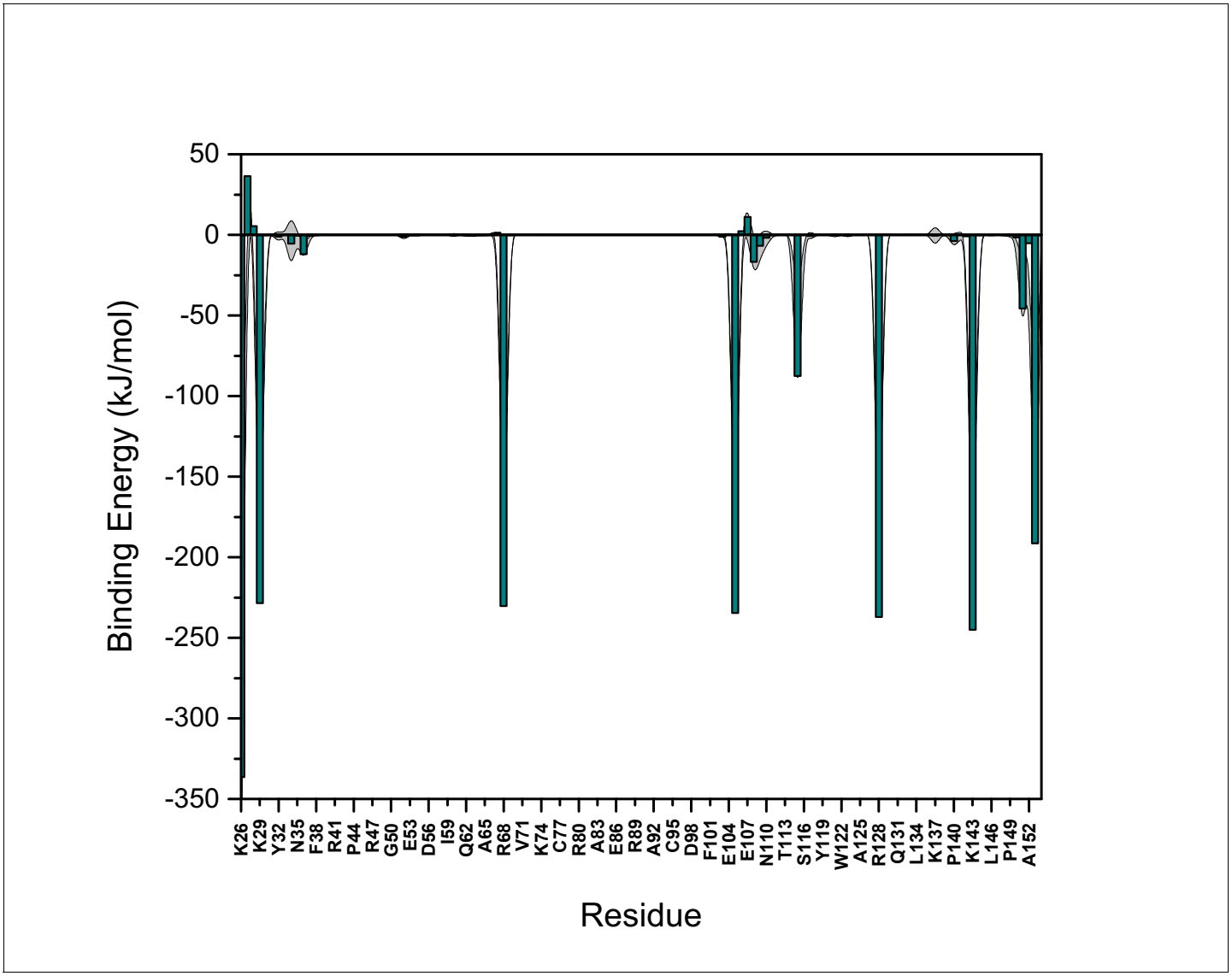

Figure 13—figure supplement 5. PI(4,5)P_2 binding energy based on electrostatics and van der Waals interactions. The average interaction energy (electrostatic and van der Waals contributions) of PI(4,5)P_2 in system M1 over the residues of FGF2 in the low-affinity orientation binding to PI(4,5)P_2. The standard errors are shown as shadows.

DOI: 10.7554/eLife.28985.025

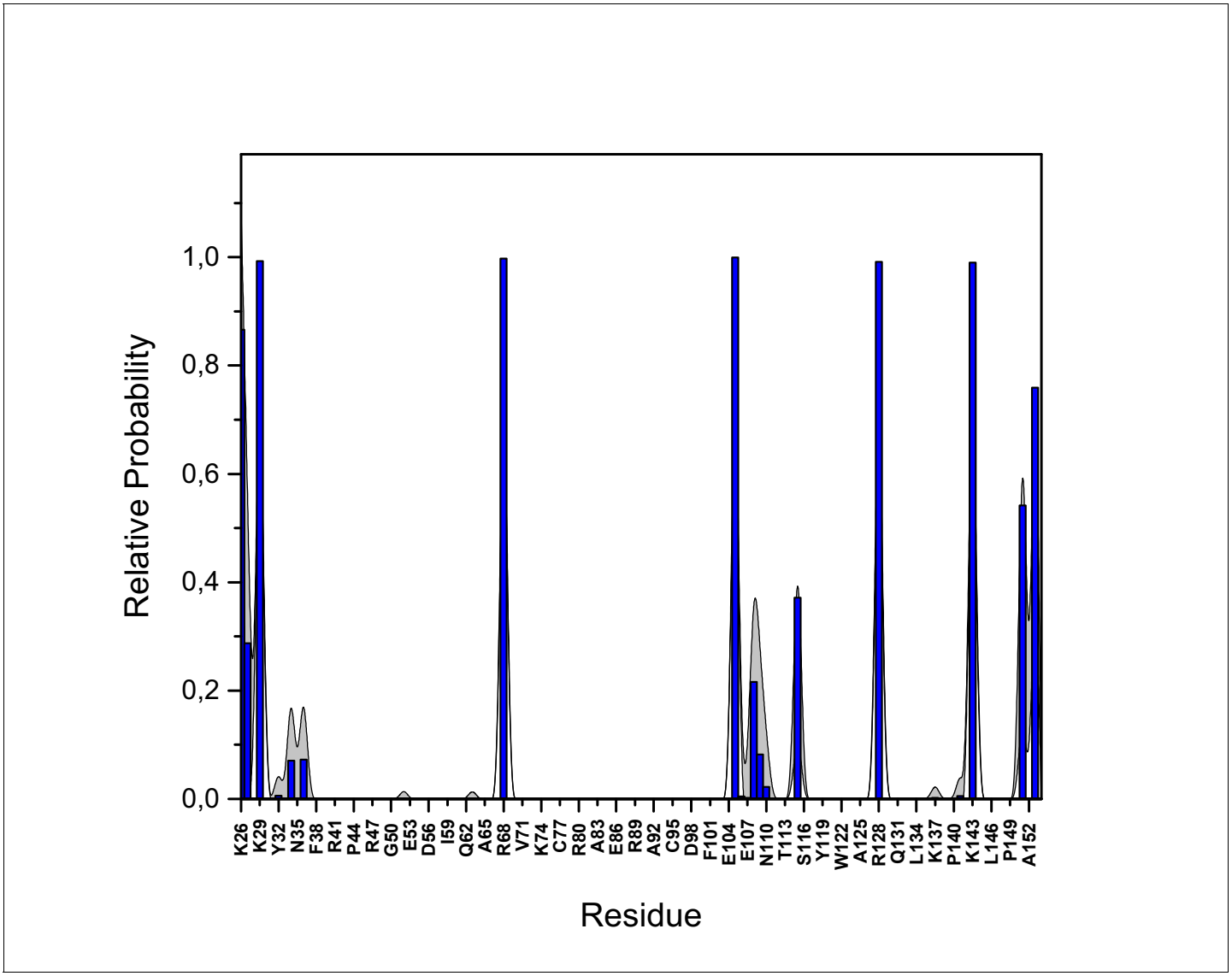

Figure 13—figure supplement 6. PI(4,5)P_2 interaction based on hydrogen bond analysis. Relative probability of hydrogen bonds formed between the residues of FGF2 in the low-affinity orientation and PI(4,5)P_2 (system M1). The standard errors are shown as shadows.
DOI: 10.7554/eLife.28985.026

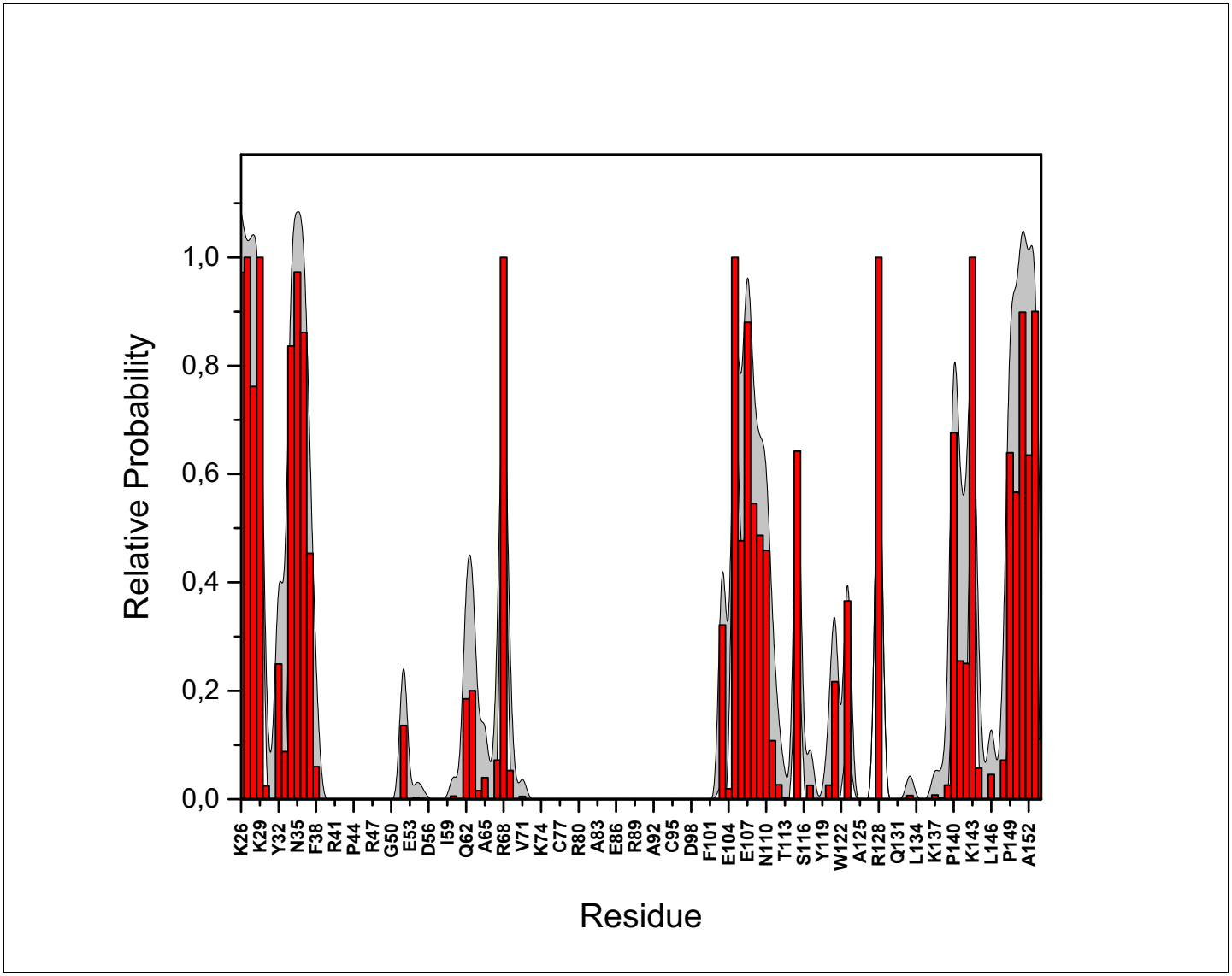

Figure 13—figure supplement 7. PI(4,5)P_2 contacts with FGF2. Relative probability of contacts (<0.6 nm) between the FGF2 residues and PI(4,5)P_2 in the low-affinity orientation (system M1). The standard errors are shown as shadows.
DOI: 10.7554/eLife.28985.027

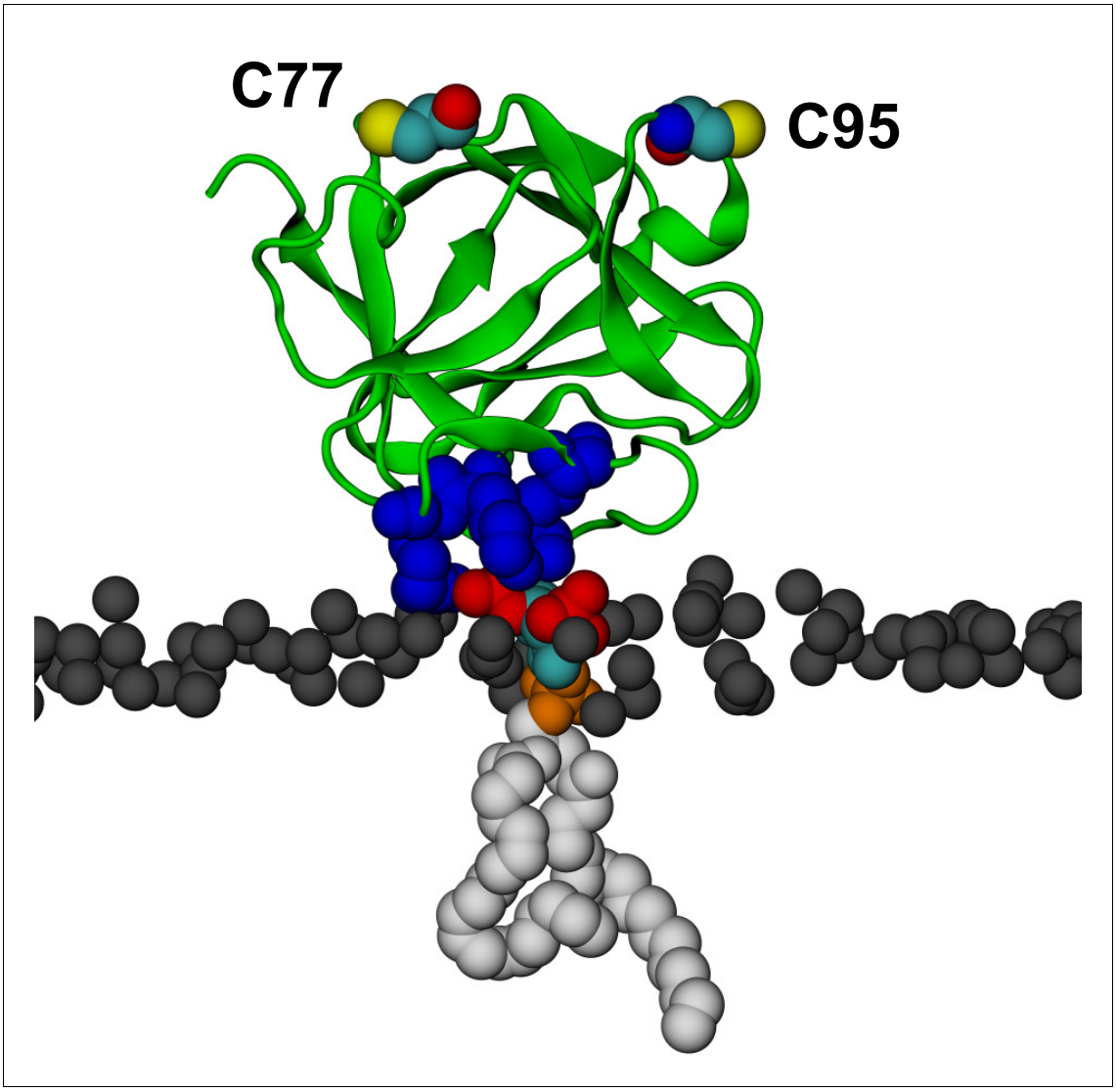

Figure 13—figure supplement 8. Binding of FGF2 to a single PI(4,5)P_2. Binding of FGF2 to a single PI(4,5)P_2 molecule (system M2) with its known binding site residues (K127, R128, K133) colored as blue van der Waals spheres. During the simulation the orientation of FGF2 in respect to the membrane fluctuated between the high-affinity (shown here) and low-affinity orientations. Color coding as in ***Figure 13***.
DOI: 10.7554/eLife.28985.028

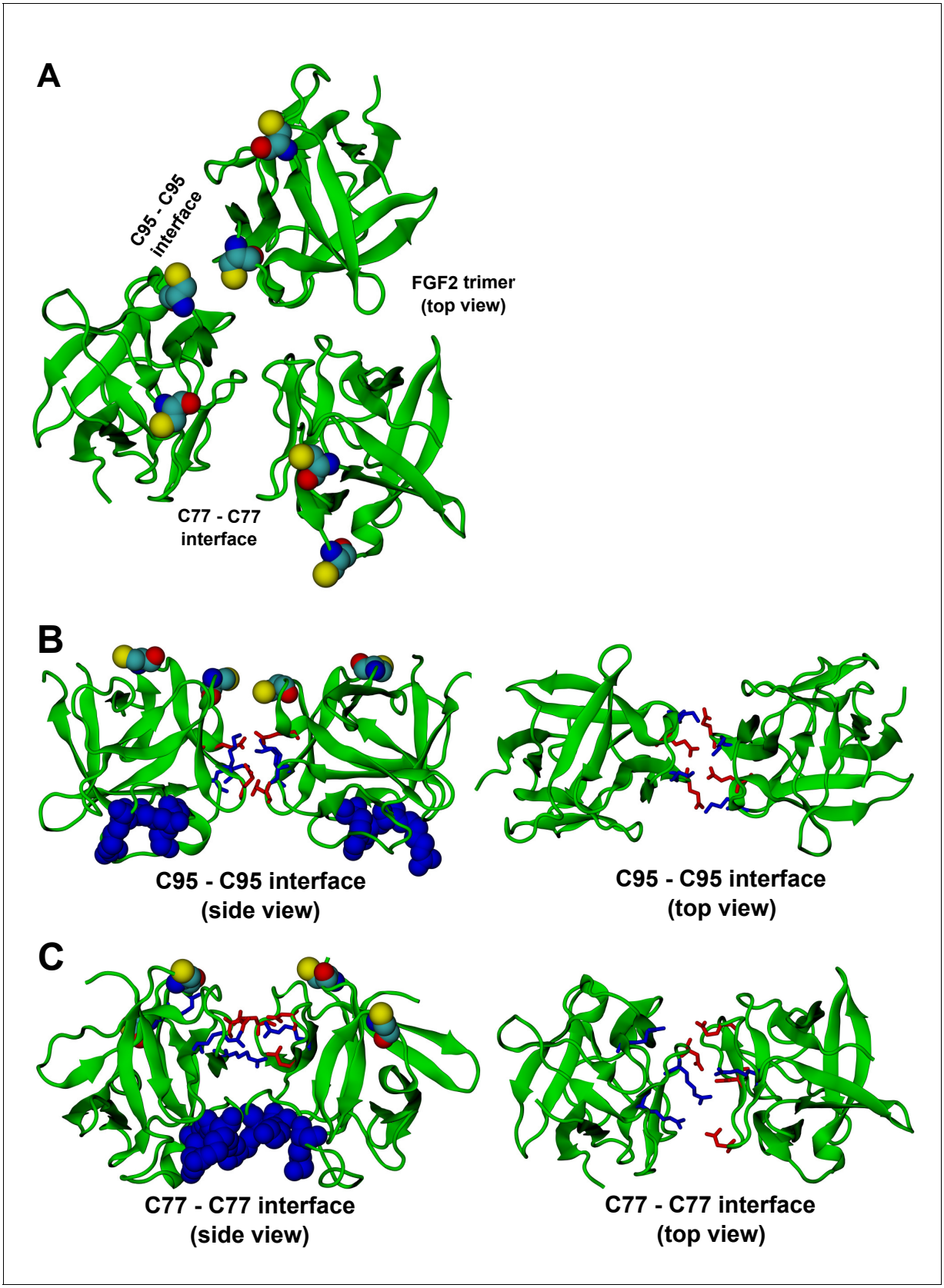

Figure 14. FGF2 trimer configurations. Snapshots representing the most populated structures in FGF2 trimer simulations (system T). (Panel **A**) depicts the top view of the FGF2 trimer aggregate with C95 – C95 and C77 – C77 interfaces labeled, where C95 and C77 are colored as van der Waals spheres.

Figure 14 continued on next page

Figure 14 continued

The trimer is split into two dimer interfaces shown in (panels **B** and **C**). (**B**) The interface residues involved in C95 – C95 disulfide-linked dimers. (**C**) The interface residues involved in C77 – C77 disulfide-linked dimers. The interface residues are depicted in stick representation, where negatively charged residues (D, E) are colored as red and positively charged residues (K, R) as blue. The $PI(4,5)P_2$ binding pocket residues (K127, R128, K133) are rendered as blue van der Waals spheres. For clarity, POPC, $PI(4,5)P_2$, cholesterol, water, and ions are not shown.

DOI: 10.7554/eLife.28985.029

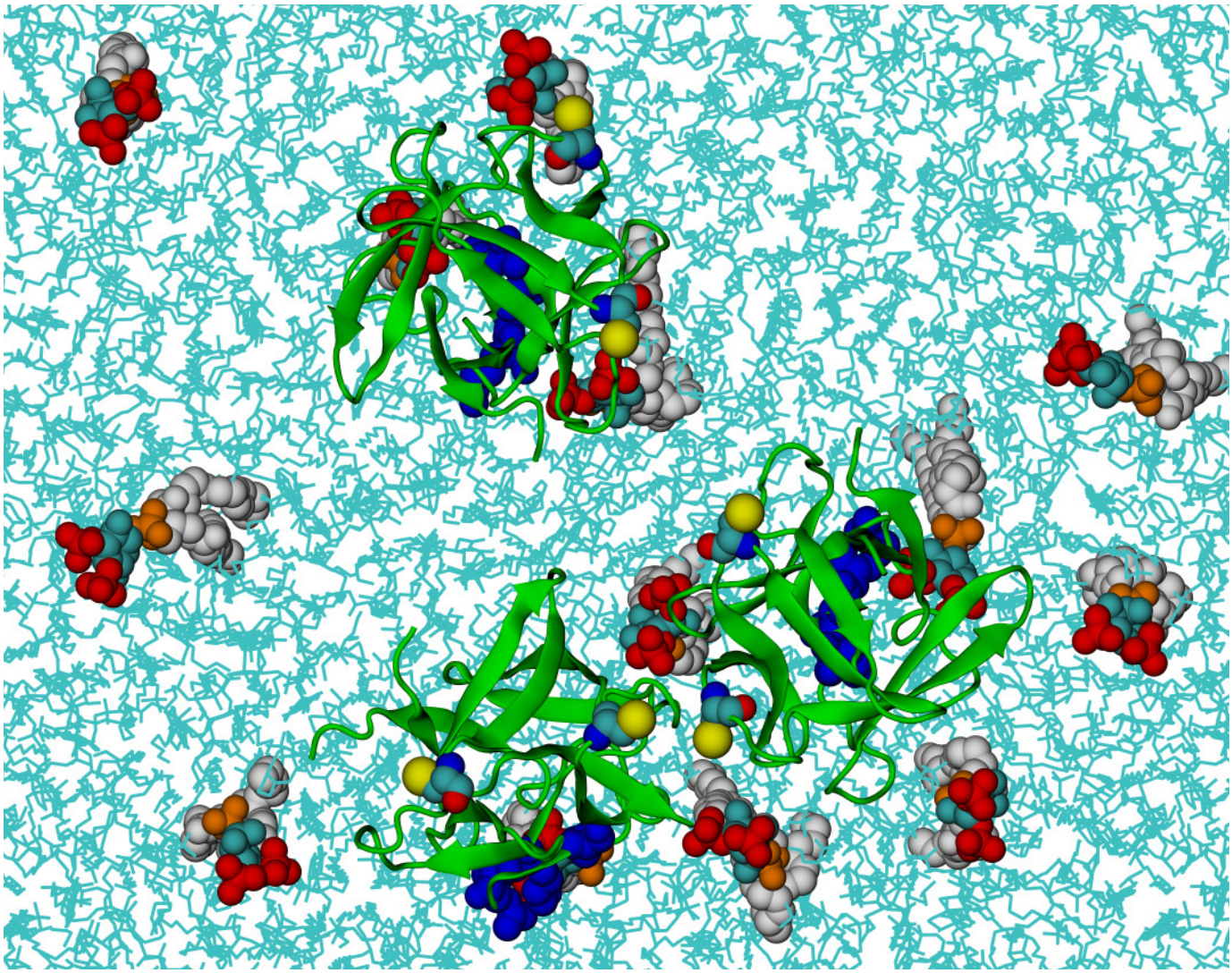

Figure 14—figure supplement 1. FGF2 trimer in the beginning of the simulations. Top view of the initial positions of three FGF2 monomers on the membrane surface in a simulation of FGF2 trimers (system T). POPC and cholesterol molecules are colored as cyan lines. The color coding of the proteins and $PI(4,5)P_2$ is as in ***Figure 13***.

DOI: 10.7554/eLife.28985.030

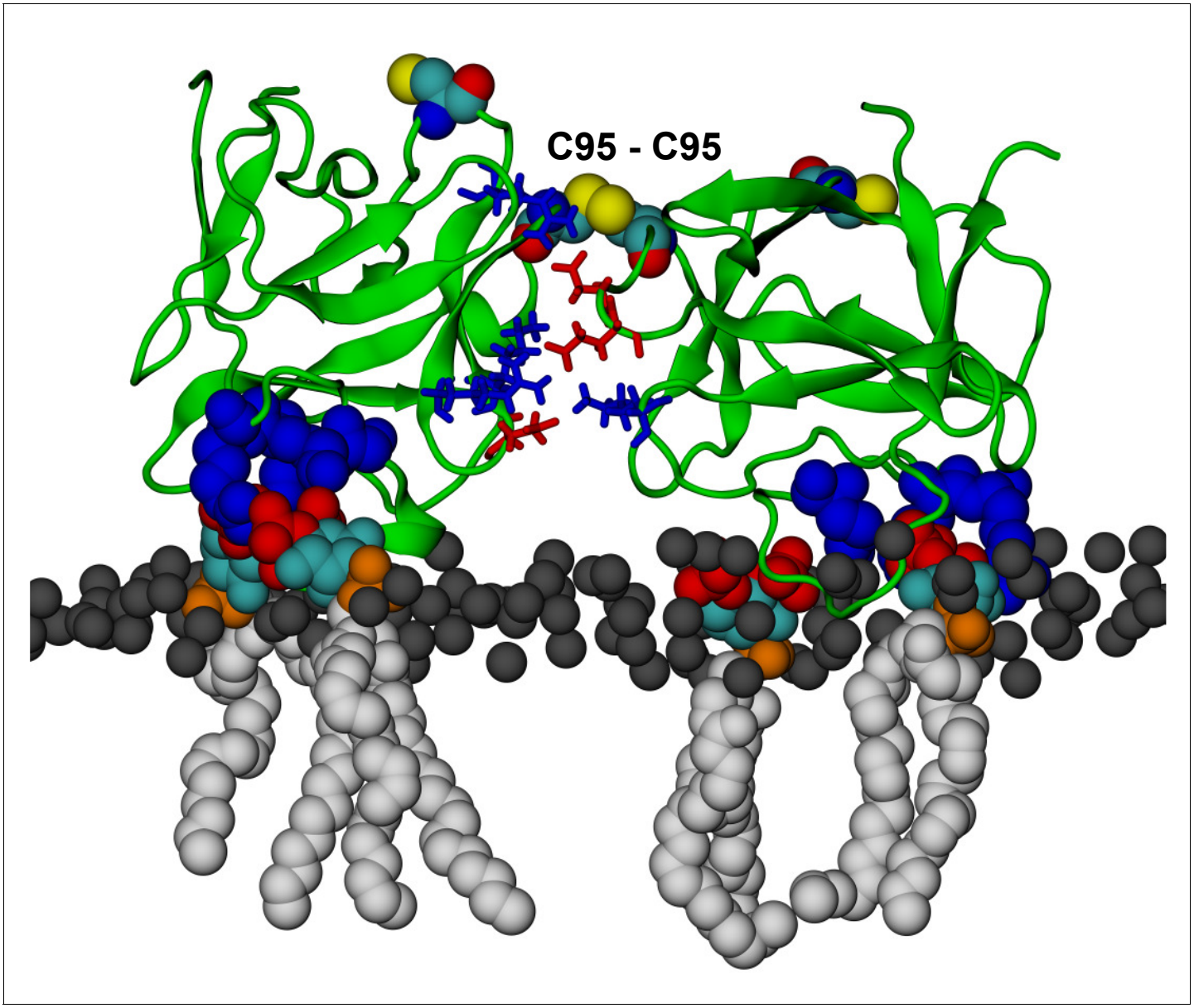

Figure 14—figure supplement 2. FGF2 dimer simulation. FGF2 dimer with a covalently linked C95 – C95 bridge (system D). C95 and C77 are shown as van der Waals spheres. The interface residues involved in ion pairs are shown in stick representation, where negatively charged residues (D, E) are colored as red and positively charged residues (K, R) as blue. The PI(4,5)P_2 binding pocket residues (K127, R128, K133) are depicted as blue van der Waals spheres. The rest of the protein and membrane is colored as in ***Figure 13***.

DOI: 10.7554/eLife.28985.031

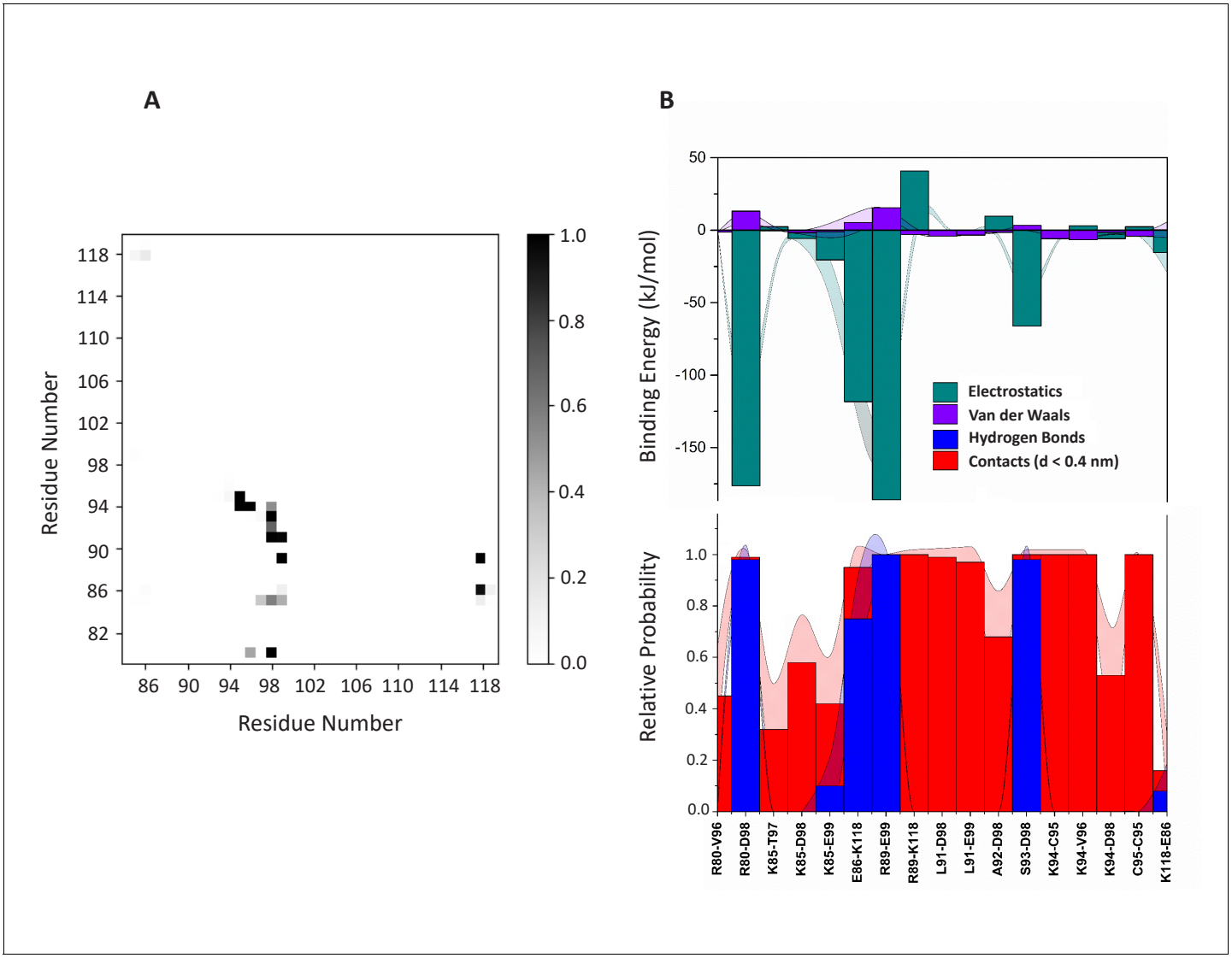

Figure 14—figure supplement 3. Dimerization interface. (**A**) Contact map analysis for the dimer (system D). (**B**) Based on the contact map, 17 residue pairs (distance <0.4 nm) were identified for which electrostatic and van der Waals interactions (panel B (top)) were computed. The hydrogen bonds and contacts are shown in panel B (bottom). The standard error is shown as shadows.

DOI: 10.7554/eLife.28985.032